Quantum Dynamics & Excitations of Ultracold Atomic Gases in Optical Lattices

Diploma Thesis

Markus Hild

July 2005

In Andenken an
Hans-Rudolf Hild
(1950-1999)

Summary

In this work ultracold atomic gases in one-dimensional optical lattices are studied in the framework of the Hubbard model. We investigate the dynamical behaviour of both, Bose gases and two-component Fermi mixtures, by performing an exact time-evolution while perturbing the system. The response is measured by evaluating several observables during the evolution, mainly in the strongly repulsive regime.

To this end, we give a short historical overview on the realisation of Bose-Einstein condensation and introduce briefly the field of ultracold gases in optical lattices. We review the Bose-Hubbard model and introduce the Hamilton operators for Bose gases and two-component Fermi mixtures. Moreover, several observables for both systems are discussed in view of the superfluid to Mott-insulator phase transition.

The time-evolution of quantum systems is discussed in general and the technical details in order to evolve Hubbard systems are outlined. Since we perform simulations of atomic gases in amplitude modulated lattice potentials, we derive the according time-dependent parameters of the Hubbard model. Furthermore, we discuss the mechanisms of particle-hole excitation which occur in the strongly repulsive regime.

We perform time-evolutions for Bose and Fermi gases with two different kinds of perturbation in order to investigate the excitation spectrum: as a stationary perturbation we apply linear potential gradients of different strengths. The system shows a continuous excitation spectrum in the weakly repulsive regime, whereas at strong interactions narrow resonances appear. These results are in good agreement with the particle-hole excitation picture. As a dynamic perturbation we simulate the behaviour of atomic gases in amplitude modulated optical lattices. We present several simulations with different system sizes, filling factors of the lattice, and boundary conditions. The resonance structure resulting from this perturbation is more complex than in the case of the gradient. We observe an additional fine-structure which seems to be beyond the simple particle-hole excitation picture.

Contents

1 Introduction *1*

2 Hubbard Model *7*

2.1 Atomic gases in optical lattices 7

2.2 The Bose-Hubbard Model 9

2.2.1 Number State Basis 9

2.2.2 Bose-Hubbard Hamiltonian 10

2.2.3 Observables 12

2.3 The Fermi-Hubbard Model 21

2.3.1 Number State Basis 21

2.3.2 Fermi Hubbard Hamiltonian 23

2.3.3 Observables 24

3 Time Evolution *27*

3.1 General Notes 27

3.2 Bose-Hubbard Model 29

3.2.1 Excitation of Atoms in Optical Lattices 30

3.2.2 Tilted Lattices 32

3.2.3 Modulated Lattice Potential 33

3.3 Methods 36

3.3.1 Crank-Nicholson scheme 37

3.3.2 Runge-Kutta methods 39

4 Bosons *41*

4.1 Tilted Lattice Potential 41

4.2 Modulated Lattice Potential 46

5 Fermions *65*

5.1 Tilted Lattice Potential 65

5.2 Modulated Lattice Potential 68

Chapter 1

Introduction

Quantum theory is the theory which describes nature on a microscopic scale. It required some experimental skill to reveal macroscopic quantum phenomena, like superconductivity found by *Heike Kammerlingh-Onnes*[1] in 1911. He observed the vanishing of the resistance of mercury below the temperature of 4.2 K. Onnes assumed, that the explanation of this phenomenon requires the quantum theory, which was in an early stage at that time. Another macroscopic quantum effect is superfluidity, which was found by Kapitsa, Allen, and Misener in 1937: They observed liquid helium ^{4}He flowing without friction below a critical temperature.

Both effects are connected to a phenomenon called Bose-Einstein condensation, which was originally conceived by *Albert Einstein* in 1925. Initiated by the studies of *Satyendra Nath Bose* on the statistics of photon gases, Einstein predicted the phase transition of a dilute gas of atoms into a special state, if cooled below a critical temperature. In this special state – the Bose-Einstein condensate – all atoms are in the same single-particle state. Particles of that kind are called *bosons* and they obey the Bose-Einstein statistics. The many-body wavefunction of bosons is symmetric under exchange of two particles, which means the wavefunction does not change. On the other hand, particles, whose wavefunction is anti-symmetric under parti-

[1] Heike Kammerlingh-Onnes received the Nobel prize of physics in 1913 "for his investigations on the properties of matter at low temperatures which led, inter alia, to the production of liquid helium". (taken from `http://nobelprize.org/physics/laureates/1913/index.html`)

cle exchange, are called fermions. They obey the Fermi-Dirac statistics. The anti-symmetry under particle-exchange implies, that two identical fermions must not be in the same state: Assuming two fermions to be in the same state, the interchange of these particles can not lead to the required sign-change of the wavefunction. This is known as the Pauli exclusion principle. Therefore, a phenomenon like the collective condensation of all particles into the same state is not possible for fermions. The symmetry of the many-body wavefunction is connected to the spin of the particles via the *spin-statistics-theorem*. Particles, whose spin is an integer multiple of the Planck constant $\hbar$ are bosons, whereas particles with half-integer multiples of $\hbar$ are fermions.

The observation of the Bose-Einstein condensate (BEC) proved to be more difficult, since liquid ^{4}He is a complex interacting system, instead of a the dilute gas as in Einsteins theory. London proposed the superfluid state of ^{4}He as a manifestation of the Bose-Einstein condensate in 1938 [1]. The evidence for a condensate in liquid helium has been established in 1995 by neutron scattering.

The experimental goal was to create a pure Bose-Einstein condensate from a dilute atomic gas as theoretically predicted by Einstein. In the beginning 1980s several groups tried to generate a pure condensate of hydrogen, which was cooled close to the transition point, but the recombination to molecules inhibited the condensation.

The most successful technique to generate a pure Bose-Einstein condensate is the combination of laser and evaporative cooling in magnetic traps. Laser cooling was invented by Steven Chu, Claude Cohen-Tannoudji, and William D. Phillips and honoured with the Nobel prize in physics in 1997. The preferred atoms to be cooled by this technique are alkalis, since their optical transitions match the wavelengths of current laser systems. Moreover, these atoms can be kept in magnetical traps at low field strengths, due to their large magnetic moments. Condensation cannot be achieved by laser cooling alone; the sample can be cooled far below the temperature needed, but the condensation requires also high densities, at which the sample simply absorbs the photons. Thus, in a second stage, the sample is kept in a magnetic trap and cooled further by evaporation. This technique is similar to cooling coffee: one allows the "hottest" atoms to leave the ensemble whereby the average temperature of the sample decreases. The only drawback is, that the number of atoms is reduced, but by this method the condensation of 2000

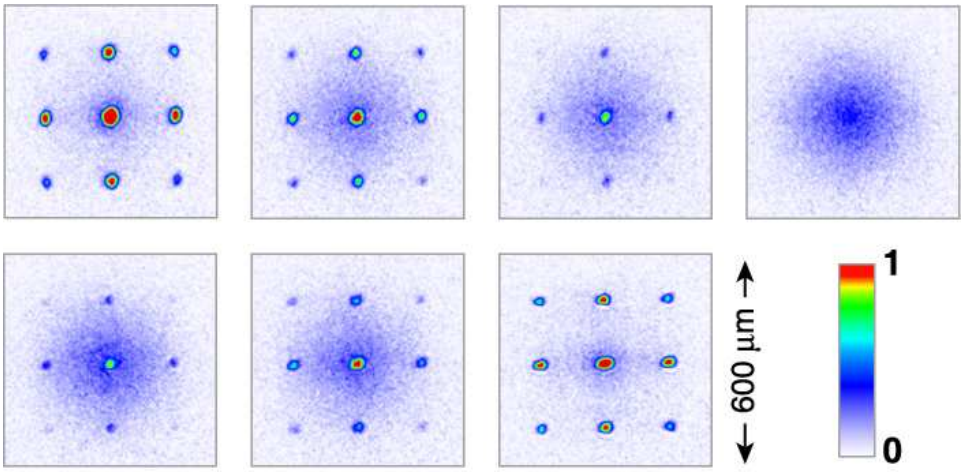

Figure 1.1: The image shows the matter-wave interference of a ultracold Bose gas in a three dimensional lattice with about 100.000 occupied sites. The sequence shows the phase-transition from the superfluid phase (upper left image) to the Mott-insulator phase with a complete loss of phase coherence (upper right image). The sequence ends by the transition back into the superfluid phase with restored phase coherence. (Taken from `http://www.physik.uni-mainz.de/quantum/bec/gallery/index.html`)

^{87}Rb atoms (rubidium) was achieved in 1995 by Eric Cornell and Carl Wieman [2] et al. (JILA). Four months later Wolfgang Ketterle et al. (MIT) observed the condensation of a sample of 5×10^5 ^{23}Na atoms (sodium) [3]. These experiments have been repeated by several groups with different alkali atoms, and in 2001 Cornell, Wieman, and Ketterle received the Nobel prize for their discoveries. The ability to create this *new kind of matter* opened whole new range of possibilities to study quantum phenomena.

In 1998 Jaksch et al. proposed the observation of another phase transition of a BEC in a optical lattice [4]. This optical lattice is generated by two counter-propagating lasers, which form a standing wave. The laser frequency is far detuned from resonances of the atoms, and due to the induced dipole force they gather in the minima or maxima (depending on the detuning relative to the atom resonance) of the standing wave. The physics of these systems is characterised by the ratio of the on-site interaction strength (U) and the strength of tunnelling (J) between the sites. The key feature is that this ratio is controlled by the intensity of the lasers. For a low ratio U/J the tunnelling dominates and condensate behaves like a superfluid. On the other

hand, a high ratio U/J suppresses the mobility of the atoms in the lattice, and the interactions dominate. In a setup with one atom per site the preferred state in the strongly repulsive regime is one with each atom pinned at a single site. While increasing the ratio U/J, the former superfluid condensate has undergone a quantum phase transition to the so-called Mott-insulator.

The studies of Jaksch et al. have been performed within the Bose Hubbard model, which they proposed as the mathematical framework. Initially, the Hubbard model was conceived by John Hubbard in 1963 to describe interacting electrons in the periodic lattice of solids. In this formalism effects like the magnetic behaviour and the metal-insulator transition of solids are studied. Another application of the Hubbard model is the description of superfluid ^{4}He in Vycor[2], a porous glass. The Bose Hubbard model as well as the Hubbard Hamiltonian of a two-component Fermi gas in optical lattices are reviewed in chapter 2.

In 2001, the group of Theodor Hänsch (LMU and MPQ Garching) confirmed the Mott-insulator phase transition in experiment [5]. Figure 1.1 depicts the matter-wave interference images during the transition from the superfluid to the Mott insulating phase and back into the superfluid state. One observes the complete loss of phase coherence in the Mott-phase which is restored by the transition back in the superfluid phase.

The advantage of these systems is the possibility to study the rich physics of strongly correlated system, which is not feasible in complex systems like solids or liquids. The systems provide the possibility to convert a weakly interacting gas into a strongly correlated system in which the physics is dominated by the interaction.

In this work we study the behaviour of ultracold atomic gases subjected to an external perturbation of the lattice, in order to reveal information on the excitation spectrum especially in the region of the phase transition. A simple method to probe the excitation spectrum is to apply a linear potential gradient across the lattice [5, 6]. Qualitatively, narrow resonances have been observered at strong repulsions, whereas in the superfluid regime a continuous spectrum appears. An alternative method to excite the system is two-photon Bragg spectroscopy via an amplitude modulation of the lattice potential. In experiment [7] one observes again also a broadening of

[2] Vycor is a product of Corning Glass Works. (URL `http://www.corning.com`)

the excitation spectrum in the weakly interacting regime and rather narrow resonances for strong repulsions.

After outlining the technical details of time-evolution within the Hubbard model and discussing the basic mechanisms of excitation in chapter 3, we present the numerical simulations of Bose gases in chapter 4. We simulate the excitation of a potential gradient and a modulated lattice amplitude by performing the exact time-evolution of the perturbed systems and the evaluation of several observables in order to measure the response. Besides Bose gases in various setups like different numbers of sites, filling factors of the lattices and boundary conditions, we also simulate a two-component Fermi gas and present the results in chapter 5.

Chapter 2

Hubbard Model

In this chapter the Bose Hubbard model is reviewed. The number state basis for a single-component boson system is discussed and several observables in view of the superfluid to Mott insulatior phase transitions are reviewed. The Hubbard Hamiltonian for a two component Fermi system as well as its number state basis is introduced and the main observable will be outlined.

2.1 Atomic gases in optical lattices

The theoretical framework to describe atoms in periodic potentials is given by the Hubbard model. This model was initially applied in solid state physics to describe magnetism. In 1998 *Jaksch et al.* employed a *bosonized* version of this model to describe bosonic atoms in optical lattices at zero temperature [4].

The *Bose-Hubbard Hamiltonian* can be derived from the Hamilton operator for bosonic atoms in an external potential:

$$\begin{aligned}\hat{\mathrm{H}} = &\int \mathrm{d}x\, \hat{\psi}^{\dagger}(x) \left(-\frac{\hbar^2}{2\mathrm{m}}\nabla^2 + V_{\mathrm{lat}}(x) + V_T(x)\right) \hat{\psi}(x) \\ &+ \frac{1}{2} g \int \mathrm{d}x\, \hat{\psi}^{\dagger}(x)\, \hat{\psi}^{\dagger}(x)\, \hat{\psi}(x)\, \hat{\psi}(x)\end{aligned} \tag{2.1}$$

in which $\hat{\psi}(x)$ and $\hat{\psi}^{\dagger}(x)$ are the bosonic field operators for a given atomic state, $V_{\mathrm{lat}}(x)$ is the optical lattice potential and $V_T(x)$ is an slowly varying external potential (e.g. parabolic trapping potential). In this model contact

interaction between the atoms is assumed. The parameter of this short-range pseudopotential $g = \frac{4\pi a_S \hbar^2}{m}$ is the two-body interaction strength, where a_S denotes the s-wave scattering length. The first term of this equation is a non-interacting Hamilton operator and the second one describes the atom-atom interaction. The optical lattice potential $V_{\mathrm{lat}}(x)$ in one dimension reads

$$V_{\mathrm{lat}}(x) = V_0 \sin^2\left(\frac{2\pi}{\lambda}x\right). \tag{2.2}$$

with the wavelength λ of the laser. Assuming the atoms to be in the lowest vibrational state the field-operators $\hat{\psi}(x)^\dagger$ and $\hat{\psi}(x)$ can be expanded in the Wannier basis:

$$\hat{\psi}(x) = \sum_{i=1}^{I} w_0(x-\xi_i)\hat{a}_i \quad \text{and} \quad \hat{\psi}^\dagger(x) = \sum_{i=1}^{I} w_0^*(x-\xi_i)\hat{a}_i^\dagger, \tag{2.3}$$

with I the number of lattice sites and $\hat{a}_i$ and $\hat{a}_i^\dagger$ the annihilation and creation operators, which obey the commutator relations

$$\left[\hat{a}_i, \hat{a}_j\right]_- = \left[\hat{a}_i^\dagger, \hat{a}_j^\dagger\right]_- = 0 \quad \text{and} \quad \left[\hat{a}_i, \hat{a}_j^\dagger\right]_- = \delta_{ij}. \tag{2.4}$$

The $w_0(x-\xi_i)$ are the groundstate Wannier functions (denoted by the index 0) localised at site i. The shape of the Wannier functions, e.g. their width, is depending on the lattice potential; this is crucial when discussing the dependency of the modulated lattice and the parameters of the Hubbard Hamiltonian in section 3.2.3.

Rewriting the Hamilton operator (2.1) using the expansions above gives

$$\begin{aligned}\hat{H} = &\sum_{i=1}^{I}(\hat{a}_i^\dagger\hat{a}_{i+1} + \hat{a}_{i+1}^\dagger\hat{a}_i)\int \mathrm{d}x\; w_0^*(x)\left(-\frac{\hbar^2}{2m}\nabla^2 + V_{\mathrm{lat}}(x)\right)w_0(x-\delta)\\ &+\sum_{i=1}^{I}\hat{a}_i^\dagger\hat{a}_i\int \mathrm{d}x\; V_T(x)\,|w_0(x-\xi_i)|^2\\ &+\sum_{i=1}^{I}\hat{a}_i^\dagger\hat{a}_i^\dagger\hat{a}_i\hat{a}_i\frac{g}{2}\int \mathrm{d}x\;|w_0^4(x)|.\end{aligned} \tag{2.5}$$

For rewriting the first term nearest neighbour hopping was assumed; δ is the lattice spacing, which is assumed to be constant over the system. The second term is isolated from the first integral, Assuming that the external potential $V_T(x)$ is slowly varying on the scale of the lattice spacing δ, the

off-diagonal contributions can be neglected. In the last term only one sum over all lattice sites remains, since on-site interaction is assumed only.

In this work we are dealing with regular a lattice potential, thus the first integral in equation (2.5) is independent of the site index i. The integrals can be carried out for a given system and define the parameters of the Bose-Hubbard Hamiltonian:

$$J = \int \mathrm{d}x\, w_0(x) \left(-\frac{\hbar^2}{2\mathrm{m}} \nabla^2 + V_{\mathrm{lat}}(x) \right) w_0(x-\delta) \tag{2.6}$$

$$\epsilon_i = \int \mathrm{d}x\, V_T(x) \left| w_0(x-\delta) \right|^2 \tag{2.7}$$

$$U = g \int \mathrm{d}x\, \left| w_0(x-\delta) \right|^4. \tag{2.8}$$

The parameter J represents the *tunnelling strength*[1], ϵ_i is a site-dependent external potential and U is the *interaction strength*. The integrals leading to J and U (equations (2.6) and (2.8)) only depend on the lattice potential (as discussed, the shape of the Wannier function is also depending on the lattice potential). Consequently, the physics of the Hubbard model are driven by the ratios U/J and ϵ_i/J. With these parameters the Bose Hubbard Hamiltonian finally reads

$$\hat{\mathrm{H}} = -J \sum_i \left(\hat{\mathrm{a}}_i^\dagger \hat{\mathrm{a}}_{i+1} + \hat{\mathrm{a}}_{i+1}^\dagger \hat{\mathrm{a}}_i \right) + \sum_i \epsilon_i \hat{\mathrm{a}}_i^\dagger \hat{\mathrm{a}}_i + \frac{U}{2} \sum_i \hat{\mathrm{a}}_i^\dagger \hat{\mathrm{a}}_i^\dagger \hat{\mathrm{a}}_i \hat{\mathrm{a}}_i \,. \tag{2.9}$$

2.2 The Bose-Hubbard Model

2.2.1 Number State Basis

As discussed in the previous paragraph the Bose-Hubbard model assumes that the lattice potential is sufficiently deep to use localised single particle wave functions. This allows to describe states within the Hubbard model by the occupation number of the lattice sites. A single state in a system of I lattice sites and N particles is characterised by the I-tuple

$$\{n_1, n_2, \cdots, n_I\}$$

[1] Also called Josephson strength, termed after the british physicist Brian David Josephson (*1940), the discoverer of the Josephson effect. It describes the tunnelling of paired electrons through an thin insulating barrier between two superconductors (Josephson junction) [8]. The arrangement of a potential barrier between two wells of the optical lattice behaves similar.

with $\sum_{n=1}^{I} n_i = N$, since the number of atoms in the lattice is assumed to be constant. By running through all compositions of N bosons on I lattice sites a model space is constructed which consists of the number states

$$\big|\{n_1, \cdots, n_I\}\big\rangle = \big|n_1\big\rangle \otimes \big|n_2\big\rangle \otimes \cdots \otimes \big|n_I\big\rangle. \tag{2.10}$$

Each *ket*-vector of this *tensor product* represents a single site i with its occupation number n_i. The number states obey

$$\big\langle\{n_1, \cdots, n_I\}_\alpha\big|\{n_1, \cdots, n_I\}_\beta\big\rangle = \delta_{\alpha\beta} \qquad \text{orthonormality} \tag{2.11}$$

$$\sum_{\alpha,\beta} \big|\{n_1, \cdots, n_I\}_\alpha\big\rangle\big\langle\{n_1, \cdots, n_I\}_\beta\big| = \hat{1} \qquad \text{completeness}^2, \tag{2.12}$$

in which the sums are evaluated by running through all compositions $\{n_1, \cdots, n_I\}$ under the constraint $\sum_{i=1}^{I} n_i = N$. Since bosons are allowed to be in an equal state at the same site the dimension of this model space grows tremendously with the number of atoms and sites. For N bosons on I lattice sites the dimension is

$$D = \frac{(N+I-1)!}{N!(I-1)!}. \tag{2.13}$$

For example, for a system of 6 bosons on 6 sites $D = 462$, for the composition of 8 bosons on 8 sites $D = 6435$, and for 12 bosons on 12 sites $D = 1352078$.

2.2.2 Bose-Hubbard Hamiltonian

Before introducing the Hamilton operator we briefly discuss how operators work on the Fock space. Analogue to the number state (2.10), operators, which affect a specific site are defined. For example, an operator $\hat{\mathrm{n}}_i$ which acts on site i is defined by

$$\hat{\mathrm{n}}_i = \hat{1} \otimes \hat{1} \otimes \cdots \otimes \hat{\mathrm{n}} \otimes \cdots \otimes \hat{1} \tag{2.14}$$

in which $\hat{\mathrm{n}}$ is the i-th operator in this product. We also abbreviate (2.14) by $\hat{\mathrm{n}}_i$, in which the index i denotes the site which $\hat{\mathrm{n}}$ operates on.

The Hamilton operator of the Bose-Hubbard model in second quantisation for bosons is given by equation 2.9:

$$\hat{\mathrm{H}} = -J \sum_i \left(\hat{\mathrm{a}}_i^\dagger \hat{\mathrm{a}}_{i+1} + \hat{\mathrm{a}}_{i+1}^\dagger \hat{\mathrm{a}}_i\right) + \sum_i \epsilon_i \hat{\mathrm{a}}_i^\dagger \hat{\mathrm{a}}_i + \frac{U}{2} \sum_i \hat{\mathrm{a}}_i^\dagger \hat{\mathrm{a}}_i^\dagger \hat{\mathrm{a}}_i \hat{\mathrm{a}}_i, \tag{2.15}$$

[2] The completeness (2.12) is restricted to the model space spanned by the first energy band.

with the tunnelling strength J and the interaction strength U. The parameter ϵ_i is a site-dependent external potential, e.g. a trapping potential. The $\hat{a}_i^\dagger$ and $\hat{a}_i$ are creation and annihilation operators which obey the commutator relations

$$\left[\hat{a}_i, \hat{a}_j\right]_- = \left[\hat{a}_i^\dagger, \hat{a}_j^\dagger\right]_- = 0 \quad \text{and} \quad \left[\hat{a}_i, \hat{a}_j^\dagger\right]_- = \delta_{ij}. \tag{2.16}$$

These operators create ($\hat{a}_i^\dagger$) or remove ($\hat{a}_i$) a particle at site i in the following fashion:

$$\begin{aligned} \hat{a}_i^\dagger \left|n_1, \cdots, n_i, \cdots, n_I\right\rangle &= \sqrt{n_i + 1} \left|n_1, \cdots, (n_i + 1), \cdots, n_I\right\rangle \\ \hat{a}_i \left|n_1, \cdots, n_i, \cdots, n_I\right\rangle &= \sqrt{n_i} \left|n_1, \cdots, (n_i - 1), \cdots, n_I\right\rangle \end{aligned} \tag{2.17}$$

This allows to define the number operator $\hat{n}_i = \hat{a}_j^\dagger \hat{a}_i$, which counts the atoms at site i, and by using the commutator relations (2.16) one can rewrite the interaction part of the Hamilton operator:

$$\hat{H} = -J \sum_i \left(\hat{a}_i^\dagger \hat{a}_{i+1} + \hat{a}_{i+1}^\dagger \hat{a}_i\right) + \sum_i \epsilon_i \hat{n}_i + \frac{U}{2} \sum_i \hat{n}_i \left(\hat{n}_i - 1\right). \tag{2.18}$$

For the following discussion we assume the Hamilton operator not to be explicit time-dependent. Moreover, we consider a translational invariant lattice and leave out the external potential part of the Hamiltonian (2.18) for convenience.

As discussed earlier, the external parameter which controls the physics of the model is the ratio of U/J. For large values of U/J the (repulsive) interaction dominates over the kinetic energy and thus hopping between lattice sites is suppressed. In the number basis discussed above, the groundstate in the strongly repulsive regime is represented by the single number state

$$\left|\psi_0\right\rangle = \left|n, n, n, \cdots, n\right\rangle,$$

where $n = 1, 2, 3, \ldots$. In this state exactly n atoms are pinned at each site. By thinking of charged atoms it is obvious why this is called an *insulating* phase: since hopping between sites is completely suppressed there is no charge transport. The insulating property is driven by the particle-particle interaction; insulators of this kind are called *Mott insulators*, in contrast to *band-*, *Peierls-* or *Anderson-* insulators, in which the transport is suppressed due to particle-lattice interactions (see [9] for details). By decreasing the ratio U/J the hopping term of (2.18) cannot be neglected anymore. Hence, the groundstate consists of more than a single number state because the

inter-site hopping weakens the strong localisation of the former Mott insulator state. This delocalisation corresponds to a groundstate consisting of a *linear combination* of number states, in which number states with the atoms bunched at a single site have a much lower weight than states with all atoms distributed over the whole lattice.

While decreasing the ratio $^{U}/_{J}$ the interaction term of (2.18) gets more and more irrelevant, until in the limit $^{U}/_{J} \longrightarrow 0$ all number states are occupied. The system is called to be in a superfluid phase.

Generally, the groundstate of a Bose-Hubbard system is given by

$$\left|\psi_0\right\rangle = \sum_{j=1}^{D} c_j^{(0)} \left|\{n_1, n_2, \cdots, n_I\}_j\right\rangle, \tag{2.19}$$

in which D is the dimension of the Fock space given by (2.13) and $c_j^{(0)}$ is the coefficient of the j-th number state. These coefficients are obtained by solving the time-independent Schrödinger equation:

$$\hat{\mathrm{H}} \left|\psi_\nu\right\rangle = E_\nu \left|\psi_\nu\right\rangle,$$

in which $\left|\psi_\nu\right\rangle$ is the ν-th energy eigenstate and E_ν the corresponding energy eigenvalue. This eigenvalue problem is solved numerically by expressing the Hamiltonian (2.18) in the number basis with the matrix elements

$$\left\langle\, n_1, n_2, \cdots, n_I \,\right|\hat{\mathrm{H}}\left|\, n_1', n_2', \cdots, n_I' \,\right\rangle. \tag{2.20}$$

In order to construct this matrix one has to run over all combinations of $\{n_1, \cdots, n_I\}$ and $\{n_1', \cdots, n_I'\}$ under the constraints $\sum_{i=1}^{I} n_i = \sum_{i=1}^{I} n_i' = N$, which makes $D \times D$ matrix elements. Since nearest neighbour hopping is assumed, the number of non-zero matrix elements is only $\sim 5D$, though.

2.2.3 Observables

Mean occupation number. The groundstate and the few excited states one obtains by exact diagonalisation of the Hamilton matrix allow to evaluate several simple observables. An observable we already used in the discussion above is the average occupation number at a specific site i. It is obtained by calculating the expectation value of the occupation number operator of the i-th site:

$$\bar{n}_i = \langle\, \psi_0 \,|\, \hat{\mathrm{n}}_i \,|\, \psi_0 \,\rangle \tag{2.21}$$

With the groundstate (2.19) one can rewrite the expectation value and gets

$$\bar{n}_i = \sum_{j=1}^{D}\sum_{k=1}^{D} \left(c_j^{(0)}\right)^* c_k^{(0)} \langle\, \{n_1, n_2, \cdots, n_I\}_j \,|\, \hat{\mathrm{n}}_i \,|\, \{n_1, n_2, \cdots, n_I\}_k \,\rangle.$$

Since the Fock basis is an eigenbasis of the occupation number operator, the expectation value in the sum can be easily evaluated and by using the orthogonality of the Fock basis one arrives at

$$\begin{aligned} \bar{n}_i &= \sum_{j=1}^{D}\sum_{k=1}^{D} \left(c_j^{(0)}\right)^* c_k^{(0)} n_i^{(k)} \delta_{jk} \\ &= \sum_{j=1}^{D} \|c_j^{(0)}\|^2 n_i^{(j)} \end{aligned} \tag{2.22}$$

where the integer $n_i^{(k)}$ are the number of atoms on the i-th site of the k-th number state. For translational invariant lattices this observable will be site independent and represents the filling factor N/I.

Number variance. Another observable is the number variance at a site i which was also used in the discussion above. The number variance reveals information on the composition of the groundstate in terms of number states. In the strongly repulsive regime, i.e. for a large ratio U/J, the groundstate consists approximately of a single number state and thus the number variance will be small. In contrast, all number states contribute to the groundstate in the superfluid regime, which results in a larger number variance. The number variance at the i-th site is given by the expectation value

$$\sigma_i = \left(\langle\, \psi_0 \,|\, \hat{\mathrm{n}}_i^2 \,|\, \psi_0 \,\rangle - \langle\, \psi_0 \,|\, \hat{\mathrm{n}}_i \,|\, \psi_0 \,\rangle^2 \right)^{1/2}, \tag{2.23}$$

where the second term in the square root is the square of the occupation number at the i-th site. This means, one has to calculate the occupation number and the expectation value of the operator $\hat{\mathrm{n}}_i^2$ in order to compute the number variance σ_i of the i-th site. Although the number variance provides information to identify the phase of the system, it is not suited as an order parameter to identify the superfluid to Mott insulator phase transition [10]: as shown on the left hand side of figure 2.1, in the region of

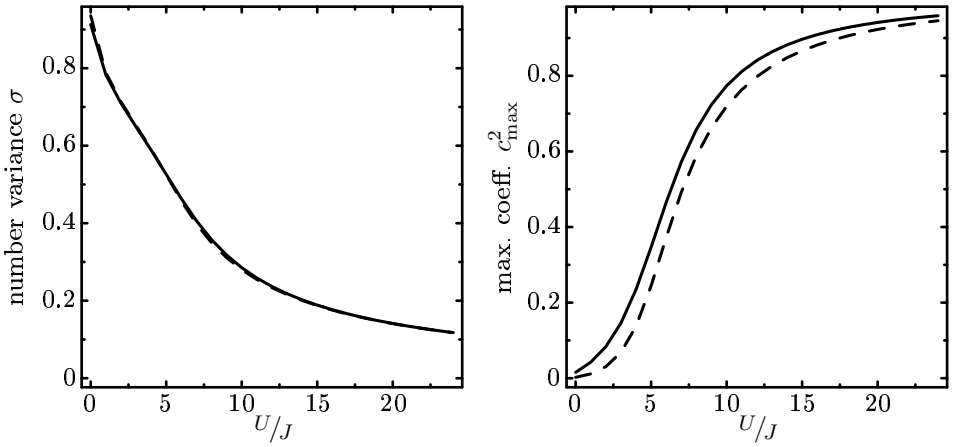

Figure 2.1: Shown are the number variance σ and the max. coefficient $C^2_{\max}$ vs. the interaction strength U of a system of 6 bosons on 6 sites (solid lines) and 8 bosons on 8 sites (dashed lines). The lattice potential is translational invariant, thus the number variance σ is site independent.

the phase transition $(U/J)_{\mathrm{cr}} = 4.65$, which was determined by Monte-Carlo calculations [11, 12], the fluctuations change linearly with the interaction strength and do not indicate a transition point.

MAXIMUM COEFFICIENT. Similar characteristics of the groundstate are revealed by the maximum coefficient

$$c^2_{\max} = \max\big(\{|c_i^{(0)}|^2\}\big) \tag{2.24}$$

of the expansion (2.19). A value $c^2_{\max} \approx 1$ indicates that the groundstate $|\psi_0\rangle$ consists of a single number state; in contrast, a small value $c^2_{\max}$ means that the state is a superposition of many number states.

ENERGY GAP. Another simple observable is the energy gap, which is a feature of the Mott insulator phase. It is defined as the energy difference between the groundstate energy E_0 and the first excited state E_1, and so it can be evaluated directly from the first two energy eigenvalues:

$$E_{\mathrm{gap}} = E_1 - E_0 \tag{2.25}$$

Figure 2.2 (left) depicts the energy of the first 50 energy eigenstates of a system of 6 bosons on 6 sites at different repulsive interaction strengths U. One

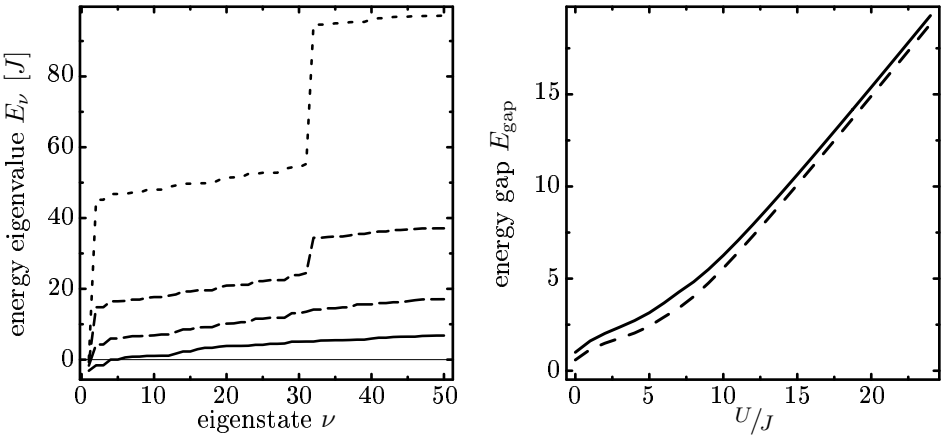

Figure 2.2: The graph on the left shows the first 50 energy eigenvalues of a system of 6 bosons on 6 sites for different interaction strengths U. The lines show the interaction strengths (bottom to top) $U = J,\ 5J,\ 20J,\ 50J$. One can see the rising energy gap between the ground and the first excited state (on the very left of the plot) in the Mott cases ($^U/_J > 4.65J$, [11, 12]). Right hand side shows the energy gap E_{gap} vs. the interaction strength U for a system of 6 bosons on 6 sites (solid line) and 8 bosons on 8 sites (dashed line).

clearly sees that several energy gaps open up at higher interaction strengths (figure 2.2). The graph on the right hand side shows the energy gap of two bosonic systems of commensurate filling factors (6 atoms on 6 sites and 8 atoms on 8 sites) versus the interaction strength U. The behaviour of a growing energy gap with increasing ratio $^U/_J$ can be explained by considering a system with commensurate filling factor, e.g. number of particles equals number of sites $N = I$. As discussed earlier in this section, for small values of $^U/_J$ the system is in the superfluid phase and all number states contribute to the groundstate. With increasing ratio $^U/_J$, the interaction between the atoms becomes more and more dominant and thus Fock states with more than one atom per site are suppressed, because they are energetically unfavourable. In the limit of an infinite interaction strength U, only the Fock state with one atom per site remains, which has a groundstate energy $E_0 = 0$. Due to admixtures of Fock states with two or more atoms per site in the first excited state and the strong interaction strength U an energy gap appears. The plot on the right of figure 2.2 shows, that the energy gap E_{gap} is increasing slowly with the interaction strength U in the superfluid phase, but in the region of the phase transition at $^U/_J \approx 5$, the slope starts

to increase up to 1 in the Mott insulator regime. This indicates that the first excited state in the Mott insulator regime is dominated by number states with exactly one doubly occupied site. Since the energy of the Fock states with one doubly occupied site is approximately U, variation of U by a certain amount changes the energy gap E_{gap} by the same amount. In contrast, for systems in the superfluid regime in which all Fock states contribute to the groundstate the energy spectrum (left hand side of figure 2.2) is rather smooth.

ENERGY TRANSFER. The energy transfer ΔE is a valuable observable in case of time-dependent Hamiltonians $\hat{\mathrm{H}}(t)$, which are utilised in chapters 4 and 5. The energy transfer ΔE is defined as the expectation value of the initial Hamilton operator $\hat{\mathrm{H}}_0 = \hat{\mathrm{H}}(t=0)$ and the current state $\big|\psi, t\big\rangle$ minus the energy of the starting state. Initial Hamilton operator means in that case, that the starting state $\big|\psi, 0\big\rangle$ is an eigenstate of $\hat{\mathrm{H}}_0$:

$$\Delta E = \big\langle\, \psi, t \,\big|\, \hat{\mathrm{H}}_0 \,\big|\, \psi, t \,\big\rangle - \big\langle\, \psi, 0 \,\big|\, \hat{\mathrm{H}}_0 \,\big|\, \psi, 0 \,\big\rangle \tag{2.26}$$

This observable provides the energy which is taken by the system under perturbation, and thus indicates excitement of the system.

CONDENSATE FRACTION. Bose Einstein condensation takes place below a specific transition temperature, if the lowest single particle energy levels are occupied. Since systems described by the Hubbard model are assumed to be at zero temperature, the condition of being lower than the transition temperature is always satisfied. In order to define a *condensate fraction* we refer on the formulation of Penrose and Onsager [13], which says that a condensate is present if one of the *natural orbitals* is *macroscopically* occupied. The natural orbitals are the eigenvectors of the *one-body density matrix* defined by the matrix elements

$$\rho_{ij}^{(1)} = \big\langle\, \psi_0 \,\big|\, \hat{\mathrm{a}}_j^\dagger \hat{\mathrm{a}}_i \,\big|\, \psi_0 \,\big\rangle \tag{2.27}$$

in which $\big|\psi_0\big\rangle$ is the given groundstate. The occupation number of a natural orbital is the corresponding eigenvalue. The macroscopic occupation is satisfied if the ratio of the occupation number and the total atom number remains finite in the thermodynamical limit ($N, I \longrightarrow \infty$ while ${}^{N}\!/_{I} = \text{const.}$). Thus, we define the condensate fraction $f_c = {}^{N_C}\!/_{N}$. From the trace of the

one-body density matrix is $\mathrm{Tr}\rho_{ij}^{(1)} = N$ follows directly, that in finite systems the largest eigenvalue is less or equal N/I. This implies that the condensate fraction is always larger than $1/I$ and remains finite.

SUPERFLUID FRACTION. Macroscopically, superfluidity is the property of a system to flow without friction. The superfluid fraction of a liquid can be defined within the two-fluid model: We consider a fluid in a tube which is moving with a velocity v. In the rest frame of the tube only the superfluid fraction of the fluid is moving. In this frame the kinetic energy of the superfluid fraction is evaluated by the difference of the energies in a system with a moving tube and one with a tube at rest. From the kinetic energy and the velocity v the superfluid fraction can be obtained.

Analogue to this macroscopic picture one can define the superfluid fraction f_s of the Bose-Hubbard system. We consider a lattice with cyclic boundary conditions, this means that the atoms can hop between the sites 1 and I directly. We force the atoms in the system to move by a velocity v_s in the lattice by a Galilei boost.

$$\left|\psi_{\mathrm{boost}}\right\rangle = \prod_{i=1}^{N} \exp\left(\frac{\mathrm{i}}{\hbar} v_s m \hat{\mathrm{x}}_i\right) \left|\psi\right\rangle, \tag{2.28}$$

in which m is the mass of a particle, N the number of particles and $\hat{\mathrm{x}}_i$ the position operator of the i-th particle. In position space the operator $\hat{\mathrm{x}}_i$ is simply the variable x_i and thus the boost operator is reduced to a phase $\exp\left(\mathrm{i}\vartheta(x_i)\right)$

$$\psi_{\mathrm{boost}}(x_1, \cdots, x_N) = \prod_{i=1}^{N} e^{\mathrm{i}\vartheta(x_i)} \psi(x_1, \cdots, x_N), \tag{2.29}$$

with the many-boson wavefunction $\psi(x_1, \cdots, x_N) = \left\langle x_1, \cdots, x_N \middle| \psi \right\rangle$ in coordinate representation. The phase $\vartheta(x_i)$ is connected to the velocity v_s via

$$v_s = \frac{\hbar}{m} \nabla \vartheta(x_i). \tag{2.30}$$

This means, that the velocity field v_s results from a spatial variation of the phase $\vartheta(x_i)$. We assume a total phase twist of θ over the length L of the lattice in the following fashion:

$$\psi(x_1, \cdots, x_k + L, \cdots, x_N) = e^{\mathrm{i}\theta} \psi(x_1, \cdots, x_k, \cdots, x_N) \;\; \forall k, \tag{2.31}$$

which is equivalent to a flow with the velocity $v_s = \frac{\hbar\theta}{mL}$. This flow is non-dissipative and irrotational which are properties of the superfluidity. Analogue to the macroscopic definition given above, the portion of the system, which follows the flow is defined as the superfluid fraction. This fraction is calculated from difference between the groundstate energies of the twisted and non-twisted systems.

In order to obtain the groundstate of the twisted system we map the unitary transformation onto the Hamiltonian. We consider

$$\hat{\mathrm{B}}_\theta = \prod_{i=1}^{N} \hat{\mathrm{U}}_{\theta,i} = \prod_{i=1}^{N} \exp\left(\frac{\mathrm{i}\theta}{L}\hat{\mathrm{x}}_i\right) \tag{2.32}$$

as the boost operator for a system of N particles. The $\hat{\mathrm{U}_{\theta,\mathrm{i}}}$ are local unitary boost operators acting on site i. The operator $\hat{\mathrm{B}}_\theta$ is not unitary, because it does not respect the cyclic boundary conditions of the Hamiltonian: we want the atoms to gain the phase θ/δ by hopping from site to site, with δ the lattice spacing; this includes also hopping between the sites 1 and I. The cyclic boundary conditions would require a phase gain of θ for this hop.

The Hamilton operator for a system with the phase twist θ reads then

$$\hat{\mathrm{H}}_\theta = \hat{\mathrm{B}}_\theta^\dagger \hat{\mathrm{H}} \hat{\mathrm{B}}_\theta \tag{2.33}$$

with $\hat{\mathrm{H}}$ the Hamiltonian of the non-twisted system. Introducing the Bose-Hubbard Hamiltonian (2.18) one gets

$$\hat{\mathrm{H}}_\theta = \hat{\mathrm{B}}_\theta^\dagger \left(-J \sum_i \left(\hat{\mathrm{a}}_i^\dagger \hat{\mathrm{a}}_{i+1} + \hat{\mathrm{a}}_{i+1}^\dagger \hat{\mathrm{a}}_i \right) + \sum_i \epsilon_i \hat{\mathrm{n}}_i + \frac{U}{2} \sum_i \hat{\mathrm{n}}_i \left(\hat{\mathrm{n}}_i - 1 \right) \right) \hat{\mathrm{B}}_\theta .$$

Since the occupation number operator does not change the position of a particle the position operator $\hat{\mathrm{x}}_j$ of the j-th particle and the operator $\hat{\mathrm{n}}_i$, which counts the atoms at site i, commute. The boost operator can be expanded in a Taylor series, which consits of powers of $\hat{\mathrm{x}}_j$, and thus it commutes with the number operator, too. This means the interaction and external potential term of the Hamiltonian are not affected by $\hat{\mathrm{B}}_\theta$ and by using the property $\hat{\mathrm{U}}_{\theta,i}^\dagger = \hat{\mathrm{U}}_{\theta,i}^{-1}$ of unitary operators one gets:

$$\hat{\mathrm{H}}_\theta = -J \sum_i \left(\hat{\mathrm{B}}_\theta^\dagger \hat{\mathrm{a}}_i^\dagger \hat{\mathrm{a}}_{i+1} \hat{\mathrm{B}}_\theta + \hat{\mathrm{B}}_\theta^\dagger \hat{\mathrm{a}}_{i+1}^\dagger \hat{\mathrm{a}}_i \hat{\mathrm{B}}_\theta \right) + \sum_i \epsilon_i \hat{\mathrm{n}}_i + \frac{U}{2} \sum_i \hat{\mathrm{n}}_i \left(\hat{\mathrm{n}}_i - 1 \right) .$$

To figure out how the boost operator (2.32) acts on the hopping term we rewrite it in a product over lattice sites instead of particles. The particles

are indistinguishable and since (2.32) affects all particles in the lattice one can express the $\hat{\mathrm{U}}_{\theta,i}$ in (2.32) by

$$\hat{\mathrm{U}}_{\theta,i} \to \hat{\mathrm{U}}'_{\theta,i} = \exp\left(\frac{\mathrm{i}\theta}{L}\xi_i\hat{\mathrm{n}}_i\right), \tag{2.34}$$

with ξ_i the coordinate of the i-th lattice site and $\hat{\mathrm{n}}_i$ the occupation number operator at site i. Therefore, the boost operator reads

$$\hat{\mathrm{B}}_\theta = \prod_{i=1}^{I} \exp\left(\frac{\mathrm{i}\theta}{L}\xi_i\hat{\mathrm{n}}_i\right). \tag{2.35}$$

As an example we evaluate the expression

$$\hat{\mathrm{B}}^\dagger_\theta \hat{\mathrm{a}}^\dagger_i \hat{\mathrm{a}}_{i+1} \hat{\mathrm{B}}_\theta = \prod_{j=1}^{I} \exp\left(-\frac{\mathrm{i}\theta}{L}\xi_j\hat{\mathrm{n}}_j\right) \hat{\mathrm{a}}^\dagger_i \hat{\mathrm{a}}_{i+1} \prod_{k=1}^{I} \exp\left(\frac{\mathrm{i}\theta}{L}\xi_k\hat{\mathrm{n}}_k\right). \tag{2.36}$$

We consider a Fock state on the right. At first the operator $\hat{\mathrm{U}}_\theta$ acts on this state and produces a product of exponential terms

$$\exp\left(\frac{\mathrm{i}\theta}{L}\xi_1 n_1\right) \cdots \exp\left(\frac{\mathrm{i}\theta}{L}\xi_j n_j\right) \exp\left(\frac{\mathrm{i}\theta}{L}\xi_{j+1} n_{j+1}\right) \cdots \exp\left(\frac{\mathrm{i}\theta}{L}\xi_I n_I\right), \tag{2.37}$$

without affecting the state itself. Then the state is changed by a hop of one particle from site $j+1$ to site j gaining the factor $\sqrt{n_j+1}\sqrt{n_{j+1}}$. Subsequently the boost operator on the left of (2.36) acts on this *new* state and creates also a product of exponential terms:

$$\exp\left(-\frac{\mathrm{i}\theta}{L}\xi_1 n_1\right) \cdots \exp\left(-\frac{\mathrm{i}\theta}{L}\xi_j (n_j+1)\right) \times$$
$$\exp\left(-\frac{\mathrm{i}\theta}{L}\xi_{j+1}(n_{j+1}-1)\right) \cdots \exp\left(-\frac{\mathrm{i}\theta}{L}\xi_I n_I\right),$$

in which n_j are the occupation numbers of the initial Fock state. These terms are almost cancelled with the previous ones, only a phase remains due to the hopping:

$$\exp\left(\frac{\mathrm{i}\theta}{L}\left(\xi_{j+1}-\xi_j\right)\right) = \exp\left(\frac{\mathrm{i}\theta}{I\delta}\delta\right) = \exp\left(\frac{\mathrm{i}\theta}{I}\right),$$

in which δ is the lattice spacing. For the second, hermitian adjoint term one gets the conjugated expression of (2.38). Finally, the Hamiltonian for twisted boundary conditions reads

$$\hat{\mathrm{H}}_\theta = -J\sum_i \left(e^{\mathrm{i}\theta/I}\hat{\mathrm{a}}^\dagger_i \hat{\mathrm{a}}_{i+1} + e^{-\mathrm{i}\theta/I}\hat{\mathrm{a}}^\dagger_{i+1}\hat{\mathrm{a}}_i\right) + \sum_i \epsilon_i \hat{\mathrm{n}}_i + \frac{U}{2}\sum_i \hat{\mathrm{n}}_i\left(\hat{\mathrm{n}}_i - 1\right), \tag{2.38}$$

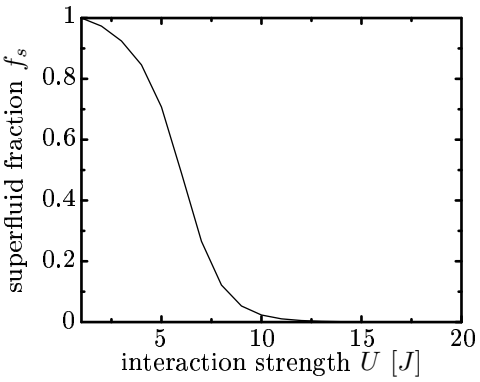

Figure 2.3: The graph shows the superfluid fraction f_s of a system of 10 bosons on 10 sites vs. the interaction strength U. In the region of the superfluid to Mott insulator phase transition ${}^{U}/_{J} \approx 5 - 8$ one can see the sharp decline of the superfluid fraction.

in which $e^{\pm \mathrm{i}\theta/I}$ are the so-called *Peierls* phase factors.

The groundstate energies of the twisted and non-twisted $E_\theta^{(0)}$ and $E^{(0)}$ system are obtained by exact diagonalisation of the Hamiltonians $\hat{\mathrm{H}}_\theta$ and $\hat{\mathrm{H}}$. The difference between these energies is the kinetic energy of the flowing superfluid:

$$E_\theta^{(0)} - E^{(0)} = \frac{1}{2} M_s v_s^2 \tag{2.39}$$

With the velocity $v_s = \frac{\hbar\theta}{mL}$ and by introducing the superfluid fraction via the mass $M_s = f_s N m$ one obtains

$$f_s = \frac{2mL^2}{\hbar^2 N} \frac{E_\theta^{(0)} - E^{(0)}}{\theta^2} \tag{2.40}$$

with m the mass of one atom, N the number of atoms and L the length of the lattice. This equation is valid for small twist angles θ. By replacing the prefactor of the kinetic energy $\frac{\hbar^2}{2m}$ by the tunnelling strength J and the length L of the lattice by the number of lattice sites I one finally gets an expression for the superfluid fraction in the lattice:

$$f_s = \frac{I^2}{JN} \frac{E_\theta^{(0)} - E^{(0)}}{\theta^2} \tag{2.41}$$

Figure 2.3 shows the superfluid fraction f_s of a system of 10 bosons on 10 sites versus the interaction strength U. The sharp decline in the region ${}^{U}/_{J} \approx 5 - 8$ indicates the phase transition between the superfluid and Mott insulator phase.

2.3 The Fermi-Hubbard Model

In this section the Hubbard model for a two-component Fermi gas is discussed. The number state basis and the Hamilton operator is introduced and the main observables are reviewed.

2.3.1 Number State Basis

Analogue to the Bose-Hubbard model (section 2.2) the lattice potential is assumed to be sufficiently deep and all atoms are in their groundstate, thus they can be described by localised Wannier functions. A composition of these single-particle states for two particle species is represented by two I-tuples

$$\{n_1^{(c)}, \cdots n_I^{(c)}\} \quad \text{and} \quad \{n_1^{(d)}, \cdots n_I^{(d)}\} \tag{2.42}$$

in which $n_i^{(c)}$ is the number of particles at site i of species c and I the number of lattice sites. Since we are describing a system of fermionic atoms which obey the Pauli exclusion principle, at most one atom of a kind is allowed at a site. Thus, the occupation numbers are restricted to $n_i^{(c)} = \{0, 1\}$. This implies that the number of atoms of a certain species cannot exceed the number of lattice sites. The model space is then constructed by all compositions (2.42) under the constraints

$$\sum_{i=1}^{I} n_i^{(c)} = N_c \leq I \quad \text{and} \quad \sum_{i=1}^{I} n_i^{(d)} = N_d \leq I \tag{2.43}$$

in which N_c is the particle number of species c. The elements of this model space are the number states

$$\left|\{n_1^{(c)}, \cdots n_I^{(c)}\}_\alpha\right\rangle \otimes \left|\{n_1^{(d)}, \cdots n_I^{(d)}\}_\beta\right\rangle. \tag{2.44}$$

This means that the model space consists of all combinations of the possible number basis states of the two species. The dimension of a single species Fock space is

$$D_c = \binom{I}{N_c} = \frac{I!}{N_c!(N_c - I)!}, \tag{2.45}$$

and thus the dimension of the Fock space of a two-component Fermi system is $D_{\mathrm{FF}} = D_c \times D_d$. For example, for a system of three fermions $N_c = 3$ and $I = 6$ lattice sites the dimension is $D_c = 20$. A Fermi-Fermi mixture

with $N_c = N_d = 3$ on 6 sites has $D_{\mathrm{FF}} = 400$. In comparison with the Bose-Hubbard model the dimension is extremly reduced due to the Pauli principle. The number state basis is also orthonormal

$$\left(\langle\{n_1^{(c)},\cdots,n_I^{(c)}\}_\alpha|\otimes\langle\{n_1^{(d)},\cdots,n_I^{(d)}\}_\beta|\right)\left(|\{n_1^{(c)},\cdots,n_I^{(c)}\}_\gamma\rangle\otimes|\{n_1^{(d)},\cdots,n_I^{(d)}\}_\delta\rangle\right) = \delta_{\alpha\gamma}\delta_{\beta\delta} \tag{2.46}$$

and complete

$$\sum_{\alpha\beta\gamma\delta}|\{n_1^{(c)},\cdots,n_I^{(c)}\}_\alpha\rangle\otimes|\{n_1^{(d)},\cdots,n_I^{(d)}\}_\gamma\rangle\langle\{n_1^{(c)},\cdots,n_I^{(c)}\}_\alpha|\otimes\langle\{n_1^{(d)},\cdots,n_I^{(d)}\}_\delta| = \hat{1} \tag{2.47}$$

A alternative notation for a certain Fock state of a Fermi-Fermi mixture in a lattice is realised by assigning the arrows $\uparrow$ and $\downarrow$ to the species c and d:

$$|\uparrow\downarrow,\uparrow,\cdots,0,\downarrow\rangle \tag{2.48}$$

in which $\uparrow$ ($\downarrow$) denotes exactly one fermion of species c (d) at the according site. This state is equivalent to

$$|1,1,\cdots 0,0\rangle\otimes|1,0,\cdots,0,1\rangle. \tag{2.49}$$

In contrast to a bosonic system one has to use creation ($\hat{\mathrm{c}}^\dagger$) and annihilation ($\hat{\mathrm{c}}$) operators which obey the *anti*-commutator relations

$$\left[\hat{\mathrm{c}}_i,\hat{\mathrm{c}}_j\right]_+ = \left[\hat{\mathrm{c}}_i^\dagger,\hat{\mathrm{c}}_j^\dagger\right]_+ = 0 \text{ and } \left[\hat{\mathrm{c}}_i,\hat{\mathrm{c}}_j^\dagger\right]_+ = \delta_{ij} \tag{2.50}$$

and thus introduce the Pauli exclusion principle. These operators create ($\hat{\mathrm{c}}_i^\dagger$) or remove ($\hat{\mathrm{c}}_i$) a fermion of species c at site i.

$$\hat{\mathrm{c}}_i^\dagger|n_1^{(c)},\cdots,n_i^{(c)},\cdots,n_I^{(c)}\rangle\otimes|n_1^{(d)},\cdots,n_I^{(d)}\rangle = = |n_1^{(c)},\cdots,n_i^{(c)}+1,\cdots,n_I^{(c)}\rangle\otimes|n_1^{(d)},\cdots,n_I^{(d)}\rangle \tag{2.51}$$

and

$$\hat{\mathrm{d}}_i|n_1^{(c)},\cdots,n_I^{(c)}\rangle\otimes|n_1^{(d)},\cdots,n_i^{(d)},\cdots,n_I^{(d)}\rangle = = |n_1^{(c)},\cdots,n_I^{(c)}\rangle\otimes|n_1^{(d)},\cdots,n_i^{(d)}-1,\cdots n_I^{(d)}\rangle \tag{2.52}$$

In the case of any of the occupation numbers is different from $\{0,1\}$ the state is invalid and the term vanishes.

2.3.2 Fermi Hubbard Hamiltonian

Since we describe two different species a hopping term for each is necessery; the hopping part of the Fermi-Fermi Hamiltonian reads then

$$\hat{\mathrm{T}} = -J\sum_i \left(\hat{\mathrm{c}}_i^\dagger \hat{\mathrm{c}}_{i+1} + \hat{\mathrm{c}}_{i+1}^\dagger \hat{\mathrm{c}}_i\right) - J\sum_i \left(\hat{\mathrm{d}}_i^\dagger \hat{\mathrm{d}}_{i+1} + \hat{\mathrm{d}}_{i+1}^\dagger \hat{\mathrm{d}}_i\right), \tag{2.53}$$

in which $\hat{\mathrm{c}}_i^\dagger$ ($\hat{\mathrm{c}}_i$) is the creation (annihilation) operator of the first and $\hat{\mathrm{d}}_i^\dagger$ ($\hat{\mathrm{d}}_i$) for the second species. Both pairs of operators obey the anti-commutator relation (2.50). Generally, the tunneling strengths J of both species are independent, but for our purposes a single J is assumed.

Since at most one particle of a species is allowed on a certain site there is no two-body interaction within the species itself. Only the inter-species interaction contributes to the Hamiltonian. The interaction part of the Fermi-Fermi Hubbard Hamiltonian is then

$$\hat{\mathrm{V}} = U_{cd}\sum_{i=0}^{I} \hat{\mathrm{n}}_i^{(c)}\hat{\mathrm{n}}_i^{(d)} \tag{2.54}$$

where U_{cd} is the interaction strength between two fermions of species c and d, and $\hat{\mathrm{n}}_i^{(c)} = \hat{\mathrm{c}}_i^\dagger \hat{\mathrm{c}}_i$ is the number operator of species c at site i. Finally, the Fermi Hubbard Hamiltonian reads

$$\begin{aligned}\hat{\mathrm{H}}_{\mathrm{FF}} = &-J\sum_i \left(\hat{\mathrm{c}}_i^\dagger \hat{\mathrm{c}}_{i+1} + \hat{\mathrm{c}}_{i+1}^\dagger \hat{\mathrm{c}}_i\right) - J\sum_i \left(\hat{\mathrm{d}}_i^\dagger \hat{\mathrm{d}}_{i+1} + \hat{\mathrm{d}}_{i+1}^\dagger \hat{\mathrm{d}}_i\right)\\ &+ U_{cd}\sum_{i=0}^{I} \hat{\mathrm{n}}_i^{(c)}\hat{\mathrm{n}}_i^{(d)}.\end{aligned} \tag{2.55}$$

Analogue to the Bose Hubbard system in section 2.2 the energy eigenstates are obtained by solving the time-independent Schrödinger equation which means diagonalisation of the Hamilton matrix. The Hamilton matrix in number state representation consits of the matrix elements

$$\Big(\big\langle\{n_1^{(c)},\cdots,n_I^{(c)}\}_\alpha\big|\otimes\big\langle\{n_1^{(d)},\cdots,n_I^{(d)}\}_\beta\big|\Big)\hat{\mathrm{H}}_{\mathrm{FF}}\Big(\big|\{n_1^{(c)},\cdots,n_I^{(c)}\}_\gamma\big\rangle\otimes\big|\{n_1^{(d)},\cdots,n_I^{(d)}\}_\delta\big\rangle\Big) \tag{2.56}$$

The diagonalisation provides the energy eigenstates

$$\big|\psi_\nu\big\rangle = \sum_{\alpha=1}^{D_c}\sum_{\beta=1}^{D_d} c_{\alpha\beta}^{(\nu)}\,\big|\{n_1^{(c)},\cdots n_I^{(c)}\}_\alpha\big\rangle\otimes\big|\{n_1^{(d)},\cdots n_I^{(d)}\}_\beta\big\rangle \tag{2.57}$$

with $c_{\alpha\beta}^{(\nu)}$ the coefficients of the i-th energy eigenstate.

2.3.3 Observables

Generally, the observables are defined in the same manner as in the Bose-Hubbard model. Here, they are briefly reviewed in terms of a two-component Fermi system.

MEAN OCCUPATION NUMBER. The mean occupation number at site i of species c is defined as the expectation value of the according occupation number operator:

$$\bar{n}_i^{(c)} = \langle\, \psi_0 \,|\, \hat{\mathrm{n}}_i^{(c)} \,|\, \psi_0 \,\rangle. \tag{2.58}$$

$|\psi_0\rangle$ is an arbitary state of the system, e.g. an eigenstate (2.56), and $\hat{\mathrm{n}}_i^{(c)}$ is the occupation number operator of species c counting the number of atoms at site i. In contrast to the pure boson system the mean occupation number of the system is in the interval $\bar{n}_i^{(c)} = (0-1)$ due to the Pauli principle. In case of an translational invariant lattice the mean occupation number is site-independent $\bar{n}_i^{(c)} = {}^{N_c}/_{I}$.

NUMBER VARIANCE. Due to the Pauli principle the number variance does not provide much information on Fermi systems. It is defined for species c at site i by

$$(\sigma_i^{(c)})^2 = \langle\, \psi_0 \,|\, \left(\hat{\mathrm{n}}_i^{(c)}\right)^2 \,|\, \psi_0 \,\rangle - \langle\, \psi_0 \,|\, \hat{\mathrm{n}}_i^{(c)} \,|\, \psi_0 \,\rangle^2, \tag{2.59}$$

The number operator $\hat{\mathrm{n}}_i^{(c)}$ acts on states with occupation numbers $n_i^{(c)} = \{0, 1\}$ only which implies that $(\hat{\mathrm{n}}_i^{(c)})^2 = \hat{\mathrm{n}}_i^{(c)}$. Thus, the site independent number variance in a translational invariant lattice is

$$(\sigma_i^{(c)})^2 = \frac{N_c}{I} - \left(\frac{N_c}{I}\right)^2. \tag{2.60}$$

In case of a non-translational invariant system the number variance is site dependent but invariant under variation of the ratio ${}^{U}/_{J}$.

CONDENSATE FRACTION. In the case of a Fermi-Fermi mixture condensation of a single species will not occur since the atoms obey Fermi-Dirac-statistics. However, the condensation of two fermions, the so-called *composite bosons*, is still possible. Especially the investigation of the phase transition from a condensate of fermion pairs to a *Bardeen-Cooper-Schrieffer* (BCS)

superfluid is currently of great interest [14, 15]. This is possible by controlling the atom-atom interactions via a magnetic-field Feshbach resonance [16]. These resonances occur at certain strengths of the magnetic field. By small variations of the field around these values one can change the interactions from attractive to repulsive and vice versa.

DRUDE WEIGHT. The analog to the superfluid fraction in the case of a bosonic system is the *Drude weight*, which characterises a transport property in fermion systems. The Drude weight is a direct probe for the metal-insulator phase transiton in a system of electrical charged fermions and thus proportional to the conductivity.

The Drude weight for a mixture of two fermionic species is defined by

$$f_D^{(c)} = \frac{I^2}{JN_c} \frac{E_\theta^{(0)} - E^{(0)}}{\theta^2}, \tag{2.61}$$

with $f_D^{(c)}$ the Drude weight of species c and N_c the number of particles. $E_\theta^{(0)}$ and $E^{(0)}$ are the groundstate energies of the twisted and non-twisted Hamiltonian. They are obtained by solving the Schrödinger equations of the non-twisted system (2.55) and

$$\hat{\mathrm{H}}_{\mathrm{FF},\theta} = -J \sum_i \left(e^{\mathrm{i}\theta/I} \hat{\mathrm{c}}_i^\dagger \hat{\mathrm{c}}_{i+1} + e^{-\mathrm{i}\theta/I} \hat{\mathrm{c}}_{i+1}^\dagger \hat{\mathrm{c}}_i \right) - J \sum_i \left(e^{\mathrm{i}\theta/I} \hat{\mathrm{d}}_i^\dagger \hat{\mathrm{d}}_{i+1} + e^{-\mathrm{i}\theta/I} \hat{\mathrm{d}}_{i+1}^\dagger \hat{\mathrm{d}}_i \right) + U_{cd} \sum_{i=0}^{I} \hat{\mathrm{n}}_i^{(c)} \hat{\mathrm{n}}_i^{(d)}.$$

which is the Fermi Hubbard Hamiltonian for a system with an external phase twist θ.

Chapter 3

Time Evolution

In this chapter the time evolution of quantum systems, especially Hubbard systems, is discussed. First, an overview over time-evolution of quantum systems in general is given. The technical details of evolving Hubbard systems as well as the basic mechanisms of excitation are discussed. Finally, different numerical methods will be outlined.

3.1 General Notes

In quantum mechanics the temporal evolution of a state is given by the time-dependent Schrödinger equation

$$\mathrm{i}\hbar\frac{\partial}{\partial t}\left|\psi,t\right\rangle = \hat{\mathrm{H}}\left|\psi,t\right\rangle, \tag{3.1}$$

where $\left|\psi,t\right\rangle$ is the time-dependent state of the system and $\hat{\mathrm{H}}$ is the Hamilton operator. In the first paragraph of this section the time-evolution of systems described by *time-independent* Hamilton operators will be discussed and the general form of a time-evolution operator will be given. We consider the initial state of the system $\left|\psi,t_0\right\rangle$ at time $t=t_0$. One possible way to derive an explicit expression for the time evolution operator is to plug the ansatz for the state $\left|\psi,t\right\rangle$ at time t

$$\left|\psi,t\right\rangle = \hat{\mathrm{U}}(t,t_0)\left|\psi,t_0\right\rangle, \tag{3.2}$$

with $\hat{\mathrm{U}}(t,t_0)$ unitary time-evolution operator, into the Schrödinger equation (3.1). This leads to a differential equation for the time-evolution operator

$\hat{\mathrm{U}}(t, t_0)$

$$\frac{\partial}{\partial t}\hat{\mathrm{U}}(t, t_0) = -\frac{\mathrm{i}}{\hbar}\hat{\mathrm{H}}\hat{\mathrm{U}}(t, t_0), \tag{3.3}$$

with the solution

$$\hat{\mathrm{U}}(t, t_0) = \exp\left(-\frac{i}{\hbar}\hat{\mathrm{H}}\int_{t_0}^{t} dt'\right).$$

For the state $\left|\psi, t\right\rangle$ follows then

$$\begin{aligned} \left|\psi, t\right\rangle &= \hat{\mathrm{U}}(t, t_0)\left|\psi, t_0\right\rangle \\ &= \exp\left(-\frac{i}{\hbar}\hat{\mathrm{H}}\,(t - t_0)\right)\left|\psi, t_0\right\rangle. \end{aligned} \tag{3.4}$$

For a given system with an Hamiltonian $\hat{\mathrm{H}}$ one has to derive the time evolution operator. For a time-independent system the most obvious way to realise this is to take advantage of the eigenbasis of the Hamiltonian $\hat{\mathrm{H}}$:

$$\hat{\mathrm{H}}\left|n\right\rangle = E_n\left|n\right\rangle \tag{3.5}$$

(time-independent Schrödinger equation) with the Eigenstates $\left|n\right\rangle$ and the energy eigenvalues E_n. The initial state $\left|\psi, t_0\right\rangle$ is expanded in the eigenbasis $\{\left|n\right\rangle\}$ by using the basis decomposition of the identity operator $\hat{1} = \sum_n \left|n\right\rangle\left\langle n\right|$:

$$\left|\psi, t\right\rangle = \sum_n \left|n\right\rangle\left\langle n|\psi, t\right\rangle = \sum_n c_n\left|n\right\rangle. \tag{3.6}$$

with the complex coefficients $c_n := \left\langle n|\psi, t\right\rangle$. Now the time evolution operator can be applied easily: in which the time-independency of $\hat{\mathrm{H}}$ was used. By introducing the expansion of the initial state (3.6) one gets

$$\left|\psi, t\right\rangle = \exp\left(-\frac{i}{\hbar}\hat{\mathrm{H}}\,(t - t_0)\right)\sum_n c_n\left|n\right\rangle,$$

where the Schrödinger equation (3.5) can be applied:

$$\left|\psi, t\right\rangle = \sum_n c_n \exp\left(-\frac{i}{\hbar}E_n\,(t - t_0)\right)\left|n\right\rangle. \tag{3.7}$$

This method requires the solution of the complete eigenproblem, which is simply not feasible for many systems: To solve the eigenproblem numerically one has to choose a basis to get the matrix representation of the Hamilton operator. This Hamilton matrix has to be diagonalised by standard numerical techniques. In many cases, one can at best compute a fraction of the eigenspectrum, due the high dimension of the problem.

In order to integrate the Schrödinger equation for systems which are not exactly solvable in terms of the aforementioned methods, one can try to solve the problem approximately. There exist a large number of numerical methods which integrate differential equations with high accuracy and performance.

The integration of *time-dependent* systems can be performed by splitting up the time interval in several small steps of Δt, in which the Hamiltonian is assumed to be constant. One has to evaluate the time-evolution operator $\hat{\mathrm{U}}(t, t_0)$ for each sub-interval in order to obtain the trajectory of the system. We apply this method in combination with a second-order approximation of the time-evolution operator for the simulations discussed in the chapters 4 and 5.

3.2 Bose-Hubbard Model

Probing the properties of ultracold atomic gases in optical lattices by using excitations has been subject of recent experimental [5, 7, 17] and theoretical [18] work. These techniques provide much information on the physics of strongly correlated systems and especially the *superfluid* to *Mott insulator phase transition* (SF-MI).

Different approaches have been employed to probe these strongly correlated systems by excitation. For instance Greiner et al. [5] examined a Bose gas in the Mott regime by applying a potential gradient. In the language of the Bose Hubbard model (equation 2.18) this corresponds to a linear increase of the energies ϵ_i across the lattice. By repeating this experiment with different linear gradients (tilts) one observes excitations at certain values. In the picture of *particle-hole excitations* these excitations occur when the energy of atoms at neighbouring sites overcomes the repulsive interaction. These sharp *resonances* are a direct indicator of the *energy gap* which indicates the presence of an Mott insulating state. Tilting was examined theoretically in [18] and is part of this work.

Another technique is the excitation by time-dependent perturbations. Stöferle et al. [7] examined the SF-MI phase transition by Bragg spectroscopy [19]. Modulation of the trapping potential with a frequency ω_{mod} adds two sidebands $\pm\omega_{\mathrm{mod}}$ relative to the laser frequency. This defines an energy difference of $\Delta E = \hbar\omega_{\mathrm{mod}}$ which in view of particle-hole excitations transfers energy to the atomic gas. This method is less sensitive to Bloch

oscillations and, unlike in lattices with linear gradients, heating of the system will not occur. Investigation of dynamical excitations of that kind are part of this work and were also investigated in [18].

In the following subsections the theoretical framework for the numerical simulation of the two techniques, tilting and modulating the lattice, are discussed.

3.2.1 Excitation of Atoms in Optical Lattices

BOSONS. This section will briefly discuss the mechanisms of excitations in the Mott regime. Basically, we assume that predominantly particle-hole excitations take place – since the atoms are separated by high barriers and the perturbations are assumed to be sufficiently low – collective excitations are neglected. The groundstate for a system of I lattice sites and $N{=}nI$ bosonic atoms ($n = 1, 2, 3, \ldots$; commensurate filling factor) in the number basis representation is approximately given by a single Fock state:

$$\big|\text{ground}\big\rangle = \big|n, n, \cdots, n\big\rangle.$$

Exciting this state in the particle-hole picture – one atom hops from the $(i+1)$-th to the i-th site – gives the normalised state

$$\begin{aligned} \big|\text{excited}\big\rangle &= \frac{1}{\sqrt{n+1}\sqrt{n}}\hat{\mathrm{a}}_i^\dagger \hat{\mathrm{a}}_{i+1}\big|\text{ground}\big\rangle \\ &= \big|n, n, \cdots, (n+1), (n-1), \cdots, n\big\rangle. \end{aligned}$$

Here, $\hat{\mathrm{a}}_i^\dagger$ and $\hat{\mathrm{a}}_i$ are the bosonic creation and annihilation operators for site i, again. Deep in the Mott regime ($U \gg J$) only the interaction term of the Bose Hubbard Hamiltonian remains:

$$\hat{\mathrm{H}} \approx \frac{U}{2}\sum_{i=1}^{I} \hat{\mathrm{n}}_i\,(\hat{\mathrm{n}}_i - 1)$$

Thus, the energy one has to provide for a hop is

$$\begin{aligned} \Delta E &= \big\langle\,\text{excited}\,\big|\,\hat{\mathrm{H}}\,\big|\,\text{excited}\,\big\rangle - \big\langle\,\text{ground}\,\big|\,\hat{\mathrm{H}}\,\big|\,\text{ground}\,\big\rangle \\ &= \frac{U}{2}\Big((I-2)n(n-1) + (n+1)n + (n-1)(n-2)\Big) - \frac{U}{2}In(n-1) \\ &= U \end{aligned}$$

Therefore, a system in the Mott regime which is perturbed by an external force can respond with a particle-hole excitation if the available energy corresponds to the interaction strength, $\Delta E = U$.

FERMI-FERMI MIXTURES. For a system of fermions one has to respect the Pauli principle which does not allow two identical fermions to be in the same state. We consider a system of I lattice sites filled with $I/2$ fermions of one species and $I/2$ fermions of a second one, denoted by '$\uparrow$' and '$\downarrow$', respectively. Furthermore, we assume strong repulsion between the two species. As discussed in chapter 2 a Fermi-Fermi system is described by a Hamilton operator (2.55) with a hopping-term for each species and an interspecies-interaction term. Again we consider the limit of strong repulsive interactions neglecting the hopping term. The Hamilton operator then reads

$$\hat{\mathrm{H}}_{\mathrm{FF}} \approx U_{\mathrm{FF}} \sum_{i=0}^{I} \hat{\mathrm{n}}_i^{\uparrow} \hat{\mathrm{n}}_i^{\downarrow}$$

In this picture the groundstate is presented by a linear combination of all Fock states with each site occupied by exactly one atom of any species. For instance, we excite the state

$$\big|\alpha\big\rangle = \big|\cdots, \underbrace{\uparrow,\downarrow}_{\text{site } i}, \cdots\big\rangle,$$

in which an arrow ($\uparrow$ or $\downarrow$) means exactly one fermion of the according type at that site. This Fock state, which is an element of the groundstate, is occupied with an atom $\uparrow$ at site i and with an atom $\downarrow$ at the neighbouring site $i+1$. All other sites are occupied with exactly one atom if any species. Because of the Pauli exclusion principle only Fermions of different states can share the same site. Therefore, only hopping to a site with an atom of different spin can occur:

$$\begin{aligned} \big|\text{excited}\big\rangle &= \hat{\mathrm{a}}^{\dagger}_{\downarrow,i}\hat{\mathrm{a}}_{\downarrow,(i+1)} \big|\alpha\big\rangle \\ &= \hat{\mathrm{a}}^{\dagger}_{\downarrow,i}\hat{\mathrm{a}}_{\downarrow,(i+1)} \big|\cdots,\uparrow,\downarrow,\cdots\big\rangle \\ &= \big|\cdots,\uparrow\downarrow,0,\cdots\big\rangle, \end{aligned}$$

with $\hat{\mathrm{a}}^{\dagger}_{\downarrow,i}$ and $\hat{\mathrm{a}}_{\downarrow,i}$ the fermionic creation and annihilation operators at site i of species $\downarrow$. The energy needed for a hop to a neighbouring site is then

$$\begin{aligned} \Delta E &= \big\langle\, \text{excited} \,\big|\, \hat{\mathrm{H}}_{\mathrm{FF}} \,\big|\, \text{excited} \,\big\rangle - \big\langle\, \alpha \,\big|\, \hat{\mathrm{H}}_{\mathrm{FF}} \,\big|\, \alpha \,\big\rangle \\ &= U_{\mathrm{FF}} - 0 = U_{\mathrm{FF}}. \end{aligned} \tag{3.8}$$

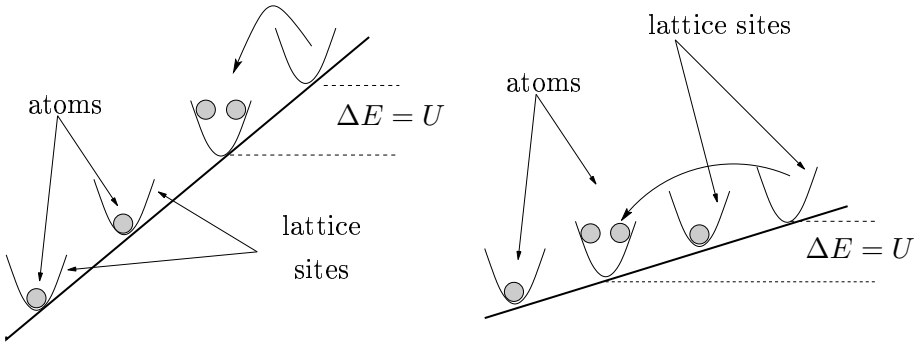

Figure 3.1: Effect of a external potential gradient: The steeper gradient enables hopping to a neighbouring site; the lower tilt enforces hopping over two sites.

Analogous to the bosons in the previous paragraph a two-component Fermi gas in an optical lattice potential will show resonant behaviour when excited with an energy $\Delta E = U_{\mathrm{FF}}$.

3.2.2 Tilted Lattices

Probing atomic gases in optical lattices by tilting the potential reveals valuable information on strongly correlated systems in experiment [5] and theory [18]. The tilting is realised by a potential gradient across the lattice. In terms of the Hubbard model, the on-site energy ϵ_i increases linearly with the site index i:

$$\epsilon_i = i\epsilon_{\mathrm{tilt}}, \tag{3.9}$$

in which i is the site index and the parameter ϵ_{tilt} controls the energy difference between neighbouring sites. If, in view of the particle-hole excitations discussed in section 3.2.1, the energy difference between neighbouring sites corresponds to the energy needed for a hop one will observe a resonant behaviour.

Besides the trivial case of hopping from site to site, next nearest neighbour hopping is also possible at lower tilting, but, since the Hamiltonians (2.18) and (2.55) do not directly connect these states, its a second order process with a lower probability. These resonance will occur at tilting $\epsilon_{tilt} = {}^{U}/_{2}$ as shown in figure 3.1. It is also possible to hop over more than two sites, but since these are processe of higher order they occur with lower probabilities.

3.2.3 Modulated Lattice Potential

The investigation of atomic gases in optical lattices by two-photon Bragg spectroscopy was subject of recent experiments [7, 20]. In contrast to applying a gradient this method is not susceptible to effects like Bloch oscillations or heating effects. Moreover, the excitation energy is tuneable very precisely. In experiment this is done by modulating the amplitude of the lattice lasers with a frequency ω_{mod}. This generates two sidebands $\pm\omega_{\mathrm{mod}}$ relative to the laser frequency which define an energy $\Delta E = \hbar\omega_{\mathrm{mod}}$.

In order to perform computer simulations of atomic gases in *modulated* optical lattices in the framework of the Hubbard model one has to account for the time-dependency of the (modulated) lattice. The one-dimensional static lattice potential reads

$$V_{\mathrm{lat}}(x) = V_0 \sin^2(kx).$$

For amplitude modulated lattices this static potential is modified by a time-dependent factor which provides the oscillation of the amplitude by a frequency ω_{mod} and a dimensionless modulation amplitude F:

$$V_{\mathrm{mod}}(x,t) = V_0 \sin^2(kx)\left(1 + F\sin(\omega_{\mathrm{mod}}t)\right). \tag{3.10}$$

In order to translate this potential into the language of the Hubbard model one has to figure out how the time-dependency of V_{mod} affects the tunnelling strength J and the interaction strength U. In analogy to the definition given in section 2.1 the time-dependent tunnelling strength is given by

$$J_{ij}(t) = \int \mathrm{d}x\; w_0\left(x-\xi_i,t\right)\left(-\frac{\hbar^2}{2m}\frac{\partial^2}{\partial x^2} + V_{\mathrm{mod}}(x,t)\right) w_0\left(x-\xi_j,t\right),$$

in which $w_0\left(x-\xi_i,t\right)$ are the Wannier-functions localised at the i-th lattice site for the lowest band (denoted by the index 0). This term gives the energy for ***hopping*** from site i to site j; only nearest-neighbour-hopping is assumed, therefore, one arrives at the simpler expression

$$J(t) = \int \mathrm{d}x\; w_0\left(x,t\right)\left(-\frac{\hbar^2}{2m}\frac{\partial^2}{\partial x^2} + V_{\mathrm{mod}}(x,t)\right) w_0\left(x-\delta,t\right), \tag{3.11}$$

in which $\delta = \xi_{i+1} - \xi_i$ is the lattice spacing. The Wannier functions are time-dependent as well – their shape depends on the lattice potential $V_{\mathrm{mod}}(x,t)$: For shallow lattice potentials it is easier for an atom to ***hop*** to an other site,

so its wavefunction will be broadened. In contrast, for deeper lattices the atom will be *pinned* to a site – its wavefunction is rather narrow.

The interaction strength

$$U(t) = \frac{4\pi\hbar^2 \mathrm{a_S}}{m} \int \mathrm{d}x \ |w_0(x,t)|^4 , \tag{3.12}$$

(with $\mathrm{a_S}$ the *s*-wave scattering length) also depends on the shape of the wavefunction and thus it depends on time because of the oscillating lattice potential.

In order to ease the solution of the integrals (3.11) and (3.12) the Wannier functions can be approximated by a Gaussian wavefunction in a harmonic potential, approximating a single well of the lattice potential (3.10) (*tight-binding* approximation):

$$\tilde{w}(x) = \frac{1}{\sqrt{\sqrt{\pi}\sigma}} \exp\left(-\frac{x^2}{2\sigma^2}\right) \tag{3.13}$$

with σ the width of the Gaussian, which depends on the lattice potential. The assumed harmonic potential is then

$$V_h(x,t) = \frac{m}{2}\left(\frac{V_0(1+F\sin(\omega_{\mathrm{mod}}t))k^2}{m}\right)x^2, \tag{3.14}$$

again, with the modulation frequency ω_{mod} and the amplitude F.

As discussed before for the Wannier functions a rather shallow lattice will result in a broader Gaussian – the parameter σ will become larger. The method to figure out this dependency, as applied in [21] and [18], is to minimise the Gross-Pitaevskii energy functional:

$$E[\tilde{w}] = \int \mathrm{d}x \ \left[\frac{\hbar^2}{2\mathrm{m}}\left|\frac{d\tilde{w}(x)}{dx}\right|^2 + V_h(x,t)\,|\tilde{w}(x)|^2 + \frac{1}{2}\frac{4\pi\hbar^2\mathrm{a_S}}{\mathrm{m}}\,|\tilde{w}(x)|^4\right] \tag{3.15}$$

Integrating this equation using the Gaussian $\tilde{w}$ (equation 3.13) with the parameter σ leads to an expression for the energy as a function of the Gaussian width

$$E[\tilde{w}] \Longrightarrow E(\sigma) = \frac{\hbar}{2\mathrm{m}}\frac{\sqrt{2}}{\sigma^2} + \frac{\mathrm{m}}{\sqrt{2}}\Omega(t)^2\sigma^2 + \frac{4\pi\hbar^2\mathrm{a_S}}{\sqrt{2\pi}\mathrm{m}\sigma}, \tag{3.16}$$

in which the abbreviation $\Omega(t) = V_0(1+F\sin(\omega t))$ was used for clarity. The stationary points of the energy functional $E(\sigma)$ are obtained by setting the derivative with respect to σ to zero:

$$\sqrt{2}\mathrm{m}\Omega^2\sigma^4 - \frac{\hbar^2}{\mathrm{m}}\sqrt{2} - \frac{4\pi\hbar^2\mathrm{a_S}}{\sqrt{2\pi}\mathrm{m}\sigma^2} = 0 \tag{3.17}$$

Solving this equation leads to an implicit expression for $\sigma(t)$:

$$\sigma^4 = \frac{\hbar^2}{m^2\Omega^2}\left(1 + 2\sqrt{\pi}\mathrm{a_S}\sigma\right) \tag{3.18}$$

This equation must be solved in order to get the width σ at a time t. As shown in [18] one can neglect the interaction part of the energy functional (3.15) and gets the simpler approximation

$$E[\tilde{w}] = \int \mathrm{d}x \left[\frac{\hbar^2}{2\mathrm{m}}\left|\frac{d\tilde{w}(x)}{dx}\right|^2 + V_h(x,t)\left|\tilde{w}(x)\right|^2\right], \tag{3.19}$$

which provides an explicit expression for the width $\sigma(t)$:

$$\sigma_{\mathrm{non-int}}(t) = \left(\mathrm{m}V_0k^2(1 + F\sin(\omega_{\mathrm{mod}}t))\right)^{-1/4} \tag{3.20}$$

Evaluating the integrals (3.11) and (3.12) using (3.20) as width of the Gaussians $\phi(t)$ leads to the equations

$$\begin{aligned} J(t) &= \frac{\hbar}{8mk^2\sigma^2}\exp\left(\frac{4k^4\sigma^4 - \pi^2}{4k^2\sigma^2}\right) \times \\ &\times \left(e^{k^2\sigma^2}(\pi^2 + 2k^2\sigma^2(V_0(1 + F\sin(\omega t))\sigma^2 - 1) - \right. \\ &- \left. 2V_0(1 + F\sin(\omega t))k^2\sigma^2)\right), \end{aligned} \tag{3.21}$$

with $\sigma = \sigma_{\mathrm{non-int}}(t)$ and

$$U(t) = \frac{2\sqrt{2\pi}\mathrm{a_S}\hbar}{\sigma(t)} = 2\sqrt{2\pi}\mathrm{a_S}\hbar\left(\mathrm{m}V_0k^2(1 + F\sin(\omega t))\right)^{1/4}. \tag{3.22}$$

After identifying the constant factor U_0 (by amplitude $F \longrightarrow 0$) from equation (3.22) one finally arrives at

$$U(t) = U_0\left(1 + F\sin(\omega t)\right)^{1/4}. \tag{3.23}$$

In case of the time-dependent expression for $J(t)$ we use the following approximation mentioned in [18] instead of implementing equation (3.21)

$$J(t) = J_0\exp(-F\sin(\omega t)). \tag{3.24}$$

This is based on the assumption of a linear dependency of the overlap of the Wannier functions in equation (3.11) with the amplitude of the lattice potential which is valid for small modulation amplitudes F.

3.3 Methods

In this section we discuss the methods used to evolve a system of atoms in periodic potentials in time. Generally, the time evolution of quantum systems is given by the time-dependent Schrödinger equation

$$\frac{\partial}{\partial t}\left|\psi,t\right\rangle = -\frac{\mathrm{i}}{\hbar}\hat{\mathrm{H}}\left|\psi,t\right\rangle \tag{3.25}$$

with the state $\left|\psi,t\right\rangle$ and the Hamilton operator $\hat{\mathrm{H}}$. Numerical calculations require to express the Hamiltonian in a basis in order to get the Hamilton matrix. The Hamilton matrix in number basis representation is a sparse matrix of a huge dimension (see section 2.1). As discussed in section 3.1 solving the Schrödinger equation (3.25) by solving the eigenvalue problem is not efficient. Especially time-dependent systems would require to diagonalise the Hamilton matrix at each timestep and thus consume lots of CPU time.

More efficient are numerical solvers for ordinary differential equations (ODEs): We employ mainly the so-called Crank-Nicholson scheme (CN), which is a mixture of the Euler explicit and implicit method and known to be unconditionally stable. Another technique is the explicit Runge-Kutta method (RK). These methods will be discussed in application to Hubbard systems and the advantages and disadvantages will be outlined.

IMPLICIT AND EXPLICIT METHODS. The Euler-methods are first order[1] methods for the integration of ordinary differential equations. In the case of the Schrödinger equation (3.25) they are given by

$$\begin{aligned}\left|\psi_{n+1}\right\rangle = &\quad \left|\psi_n\right\rangle + \tfrac{\partial}{\partial t}\left|\psi_n\right\rangle\Delta t \qquad \text{Euler explicit,}\\ \left|\psi_{n+1}\right\rangle = &\quad \left|\psi_n\right\rangle + \underbrace{\tfrac{\partial}{\partial t}\left|\psi_{n+1}\right\rangle\Delta t}_{\text{timestep}} \quad \text{Euler implicit,}\end{aligned}$$

in which $\left|\psi_n\right\rangle$ denotes the state at the n-th timestep and Δt is the size of timestep. $\hat{\mathrm{H}}(t_n)$ is the Hamilton operator at time $t_n = n\Delta t$. For instance, the equation for the explicit method means that the next state $\left|\psi_{n+1}\right\rangle$ is the current state $\left|\psi_n\right\rangle$ plus the so-called *timestep-function* $\frac{\partial}{\partial t}\left|\psi_n\right\rangle\Delta t$. The derivative inside the timestep function is given by the Schrödinger equation

[1] A solver is of order n if the error is of order $\mathcal{O}\left(\Delta t^{n+1}\right)$

(3.25) so the evolution equations finally read

$$|\psi_{n+1}\rangle = |\psi_n\rangle - \frac{\mathrm{i}\Delta t}{\hbar}\hat{\mathrm{H}}(t_n)\,|\psi_n\rangle, \tag{3.26}$$

$$|\psi_{n+1}\rangle = |\psi_n\rangle - \frac{\mathrm{i}\Delta t}{\hbar}\hat{\mathrm{H}}(t_{n+1})\,|\psi_{n+1}\rangle. \tag{3.27}$$

The difference between these two methods is that the timestep function of the explicit method can be evaluated directly using the present state and Hamilton matrix; in contrast, the implicit method involves the $(n+1)$-th state in its timestep function, which is not yet known. By rewriting equation (3.27) one gets

$$\left(\hat{1} + \frac{\mathrm{i}\Delta t}{\hbar}\hat{\mathrm{H}}(t_{n+1})\right)\,|\psi_{n+1}\rangle = |\psi_n\rangle,$$

which is a set of linear equations for the state $|\psi_{n+1}\rangle$. Thus, in order to solve an ordinary linear equation like the Schrödinger equation using an *implicit* methods one has to solve a set of linear equations in each timestep. The benefit of this effort is the better stability of these algorithms compared to explicit methods.

3.3.1 Crank-Nicholson scheme

DERIVATION. As mentioned earlier the Crank-Nicholson scheme is a mixture of the two Euler methods presented in the previous paragraph. Unlike the Euler method it is second order in time. The implicit iterative equation reads

$$|\psi_{n+1}\rangle = |\psi_n\rangle - \frac{1}{2}\left(\frac{\mathrm{i}\Delta t}{\hbar}\hat{\mathrm{H}}(t_n)\,|\psi_n\rangle + \frac{\mathrm{i}\Delta t}{\hbar}\hat{\mathrm{H}}(t_{n+1})\,|\psi_{n+1}\rangle\right), \tag{3.28}$$

which can be rewritten analogously to the implicit Euler equation into linear equations:

$$\left(\hat{1} + \frac{\mathrm{i}\Delta t}{2\hbar}\hat{\mathrm{H}}(t_{n+1})\right)\,|\psi_{n+1}\rangle = \left(\hat{1} - \frac{\mathrm{i}\Delta t}{2\hbar}\hat{\mathrm{H}}(t_n)\right)\,|\psi_n\rangle. \tag{3.29}$$

The right hand side is a matrix-vector product of known values. Equation (3.29) can be rewritten into the so-called *Caley* form of the approximation of the time-evolution operator:

$$\hat{\mathrm{U}}(t_{i+1}, t_i) = \frac{\hat{1} - \frac{\mathrm{i}\Delta t}{2\hbar}\hat{\mathrm{H}}(t_n)}{\hat{1} + \frac{\mathrm{i}\Delta t}{2\hbar}\hat{\mathrm{H}}(t_{n+1})} \tag{3.30}$$

This is the *Crank-Nicholson propagator* which evolves a state by Δt in time. Assuming that the Hamilton operator hardly changes in the time interval $[t, t + \Delta t]$ one may evaluate both Hamiltonians in equation (3.30) at the same time and gets

$$\hat{\mathrm{U}}(t_{i+1}, t_i) \to \hat{\mathrm{U}}'(t_{i+1}, t_i) = \frac{\hat{1} - \frac{\mathrm{i}\Delta t}{2\hbar}\hat{\mathrm{H}}(t_{n+1/2})}{\hat{1} + \frac{\mathrm{i}\Delta t}{2\hbar}\hat{\mathrm{H}}(t_{n+1/2})}, \tag{3.31}$$

which is a *unitary* form of equation (3.30) and thus assures the conservation of the norm of the state over time. The time $t_{n+1/2} = \Delta t(n + 1/2)$ means that the Hamiltonian is evaluated in the middle of the time interval.

NUMERICAL IMPLEMENTATION. In order to perform the time-evolution itself some preparatory work has to be done: One has to generate the hopping matrix (off-diagonal elements of the Hubbard Hamilton matrix) in number basis representation and the basis itself. In our case these are obtained by a single software package which requires the number of lattice sites, number of atom types and the number of atoms of each type. The initial state for the time-evolution is the groundstate of the Hamilton matrix consisting of the hopping matrix and a potential matrix for a certain interaction strength U (see section 2.1).

The time evolution itself starts by loading the initial state, the hopping matrix and the number basis. The hopping matrix is stored in the *compressed column format* which is required by the linear equation solver. The number basis is stored in the *basis*-object. This object allows to perform all operations needed, e.g. calculating the on-site potential and external potential part of a certain fock state as well as applying creation and annihilation operators to states.

The evaluation of various observables is also encapsulated in a class: The objects of this class must also be initialised with the system parameters.

Equation 3.29 gives the linear equations that has to be solved at each timestep. We rewrite it in the unitary form as discussed in the previous paragraph:

$$\left(\hat{1} + \frac{\mathrm{i}\Delta t}{2\hbar}\hat{\mathrm{H}}(t_{n+1/2})\right)\,|\psi_{n+1}\rangle = \left(\hat{1} - \frac{\mathrm{i}\Delta t}{2\hbar}\hat{\mathrm{H}}(t_{n+1/2})\right)\,|\psi_n\rangle. \tag{3.32}$$

The matrices on both sides of equation (3.32) differ only by the sign; in order to save memory we construct the left hand side matrix from the hopping

matrix and the potential. The right hand side of equation (3.32) is evaluated via a matrix-vector product of left hand side matrix and the current state respecting the change of sign in this operation. The set of linear equations is solved using the UMFPACK package (version 4.3) by Davis [22]. The matrices in equation (3.32) have the same structure as the Hamilton matrix in the off-diagonal-part (zero matrixelements are conserved), the diagonal part is non-zero. In contrast, due to Fock states with one or zero particles per site, the Hamilton matrix might have zeros in the potential part. Nevertheless, the sparsity of the matrix is conserved. The new state is passed to the observables object, which evaluates and stores the data. This process is repeated until the complete time-interval has been covered.

Solving the time-dependent Schrödinger equation using the combination of the Crank-Nicholson scheme and the UMFPACK sparse linear solver works very well for all our problems. The method is very stable with respect to changes in the stepsize, thus it allows a coarse analysis with a rather large timestep to get a qualitative picture.

A drawback of this and probably all implicit solving routines is the linear equation problem, which consumes lots of CPU time. For example, evolving a system of 6 bosons on 6 lattice sites (number basis dimension 462) takes about 30 seconds for 1000 timesteps; a system of 8 bosons on 8 sites (dimension 6435) takes 30 seconds per step (both on a standard PC).

Promising in that case is changing from the UMFPACK solver to the PARDISO package by Schenk et.al. [23]: This software package combines direct and iterative solvers and its performance is less dependent on the system size than UMFPACK. Additionally, the package allows parallel computing on SMP machines (multi-processor machines) with an auspicious performance gain. Although this package is not yet fully implemented in our code we were able to estimate its performance. It should be possible to examine bosonic systems up to 10 sites and 10 atoms on standard 64bit machines.

3.3.2 Runge-Kutta methods

In order to go to bigger system sizes we implemented the Runge-Kutta method as used by Braun-Munzinger [18]. As an explicit method it does not require to solve linear equations. The classical Runge-Kutta is a fourth

order method which is based on the explicit Euler method presented in this section. It gains accuracy by taking smaller trial steps instead of the full timestep and summing these up. For instance, the classical fourth order Runge-Kutta takes 4 trial steps and the summing up cancels out the lower order error terms (see [24]). Generally, the higher order of explicit methods is not sufficient keep the error small in comparison to the Crank-Nicholson method. Thus we employ the *embedded fifth order Runge-Kutta* method from *Numerical Recipes* [24], which uses an adaptive stepsize control to reduce its error. Unlike the original form of this method by *Fehlberg* [25], it is equipped with optimised *Cash-Karp* [26] parameters.

However, the algorithm did not yet perform as expected: A first explicit version of the fifth order Runge-Kutta algorithm was quite fast but also very unstable. The performance gain was lost due to the significant reduction of the step size. The embedded fifth order Runge-Kutta method with step-size control is slightly faster than the Crank-Nicholson method but it lacks accuracy in direct comparison.

Chapter 4

Bosons

In this chapter the simulations of bosonic atoms in optical lattices are presented, and different configurations of interaction strengths, filling factors and system sizes are discussed. In the first part we discuss the results for stationary pertubations of these systems by a tilted lattice potential. In the main part, the simulations of dynamic excitations via a modulated lattice potential are presented. For convenience all quantities throughout this chapter are given in natural units, that means that $c = \hbar = 1$.

4.1 Tilted Lattice Potential

In this section we present the results of a system of bosons in a tilted lattice. As discussed in section 3.2.2 tilting the lattice potential is a simple method to probe the excitation spectrum of a strongly correlated system. In terms of the Bose Hubbard model, a tilted lattice potential means, that a linearly increasing on-site energy enters the into Hamiltonian:

$$\hat{\mathrm{H}} = -J \sum_{i=1}^{I} \left(\hat{\mathrm{a}}_i^\dagger \hat{\mathrm{a}}_{i+1} + \hat{\mathrm{a}}_{i+1}^\dagger \hat{\mathrm{a}}_i \right) + \sum_{i=1}^{I} \epsilon_i \hat{\mathrm{n}}_i + \sum_{i=1}^{I} \hat{\mathrm{n}}_i (\hat{\mathrm{n}}_i - 1), \tag{4.1}$$

in which ϵ_i is a single-particle on-site energy contribution to the overall potential. The ϵ_i are defined by

$$\epsilon_i = i\epsilon_{\mathrm{tilt}},$$

where ϵ_{tilt} is the site-independent energy difference between neighbouring sites.

For a system in the Mott insulator regime $U \gg J$ we assume that excitations are adequately described in the particle-hole picture (section 3.2.1). Furthermore, the groundstate of a system of N bosons and $I = N$ lattice sites is given by

$$\big|\psi\big\rangle = \big|1, 1, 1, 1, \cdots, 1, 1\big\rangle.$$

As discussed in section 3.2.2, if the lattice tilting equals the interaction strength $\epsilon_{\text{tilt}} = U$, i.e., the external potential provides enough energy for an atom to hop *down* the tilted lattice onto another atoms site.

We simulate a system of 6 bosons with 6 lattice sites using cyclic boundary conditions, that means, atoms can hop between first and last site directly. Moreover, a certain ratio U/J is chosen, at which the simulation takes place. As initial state, the groundstate of the non-tilted Hamiltonian (4.1) is computed. In order to explore the excitation spectrum of this system we performed the time evolution for lattice tilts in the range from $\epsilon_{\text{tilt}} = 0$ to $2U$. The evolution starts with the non-tilted Hamiltonian and its groundstate. After a time $t = 0.1\ J^{-1}$ the lattice tilt is instantly applied and kept until the simulation ends at time $t = 20\ J^{-1}$. At each timestep the observables energy transfer and number variance are evaluated.

Figures 4.1, 4.2, and 4.3 illustrate the results of the simulations for systems with $U/J = 50,\ 20,$ and 10. In all figures the energy transfer is illustrated on the left hand site, and the number variance at the third site is depicted on the right of each figure. The density plots (lower plots) show the observables as function of time and lattice tilting ϵ_{tilt}, in which the magnitude of the observable is indicated by the colour scheme. The colour reaches from dark blue for lower values via green up to red for larger magnitudes. The plots above of the density plots illustrate the averaged values over the full time $t = 0$ to $t_{\text{max}}) = 20\ J^{-1}$. In both systems, resonances occur if the lattice tilting equals the interaction strength $\epsilon_{\text{tilt}} = U$ as proposed above. Moreover, resonances occur at fractional values of U, as discussed in section 3.2.1: a resonance at the lattice tilting $\epsilon_{\text{tilt}} = U/2$ indicates a hop to the next nearest neighbouring site. Additionally, in the case of $U/J = 50$ and $U/J = 20$ resonances at $\epsilon_{\text{tilt}} = U/4$ are clearly visible, which indicate hops over four sites.

In conclusion, at smaller ratios U/J the excitation spectrum is broad

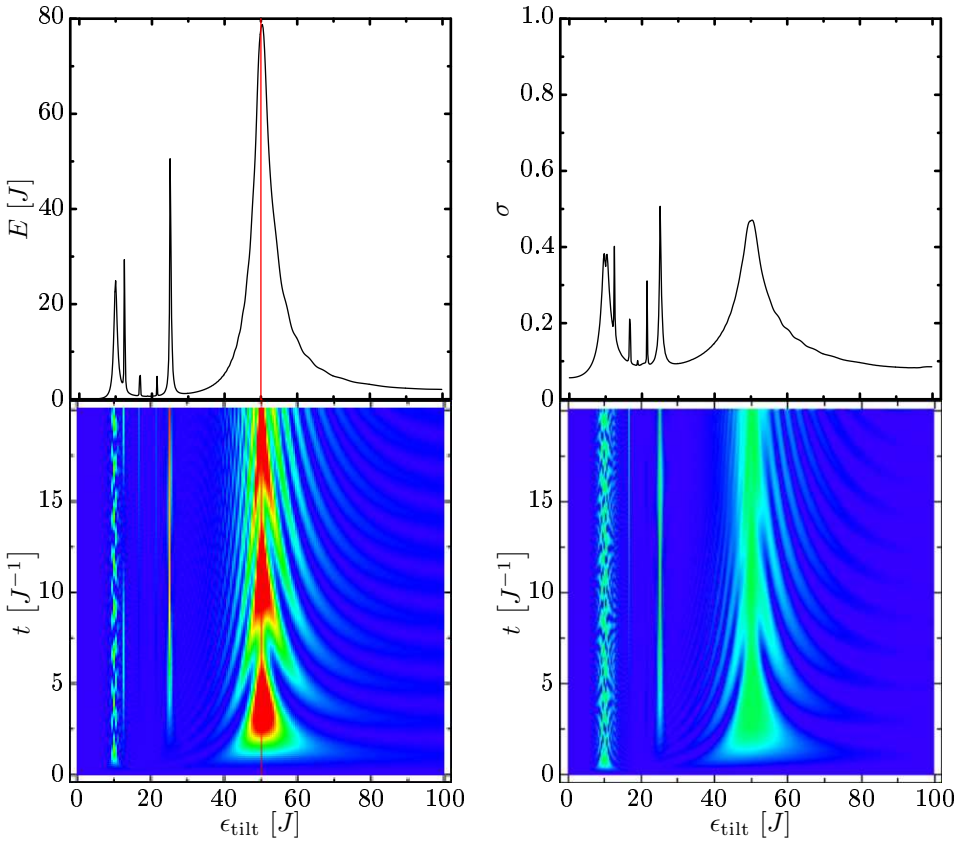

Figure 4.1: The figure illustrates a system of 6 bosons on 6 sites of a tilted lattice at the ratio $U_0/J_0 = 50$. On the left hand side the energy transfer is depicted, on the right the number variance is shown. The lower images show these observables as function of time (vertical axis) and external potential ϵ_{tilt} (horizontal axis), i.e. the potential difference between neighbouring sites. The images on top of the density plots show the time-averaged data. The red line in the energy transfer plots denotes the tilting $\epsilon_{\mathrm{tilt}} = U$.

and continuous. On the other hand, sharp peaks appear in the strongly repulsive regime, forming rather sharp resonance structure, which is in very good agreement with the picture of particle-hole excitations. The sequence of simulations with decreasing U/J (figures 4.1-4.3) shows also the rise of a background in the number variance due to the increasing mobility of the atoms.

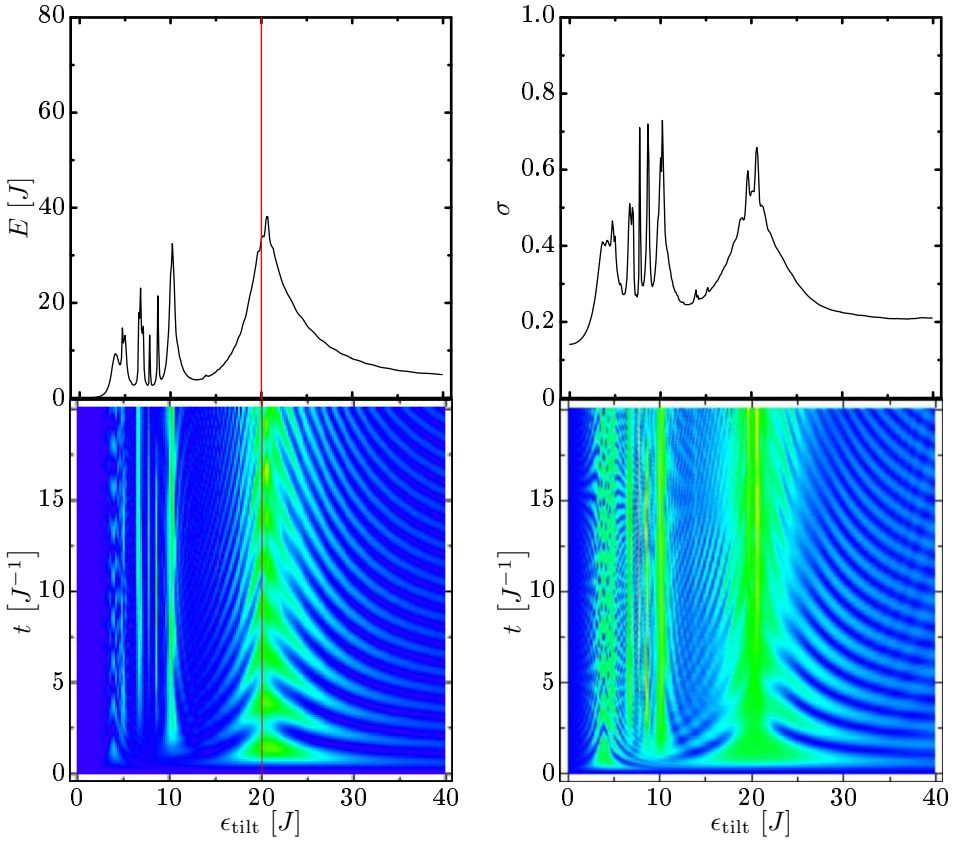

Figure 4.2: The figure illustrates a system of 6 bosons on 6 sites of a tilted lattice at the ratio $U/J = 20$. On the left hand side the energy transfer is depicted, on the right the number variance is shown. The lower images show these observables as function of time (vertical axis) and external potential ϵ_{tilt} (horizontal axis), i.e. the potential difference between neighbouring sites. The images on top of the density plots show the time-averaged data. The red line in the energy transfer plots denotes the tilting $\epsilon_{\mathrm{tilt}} = U$.

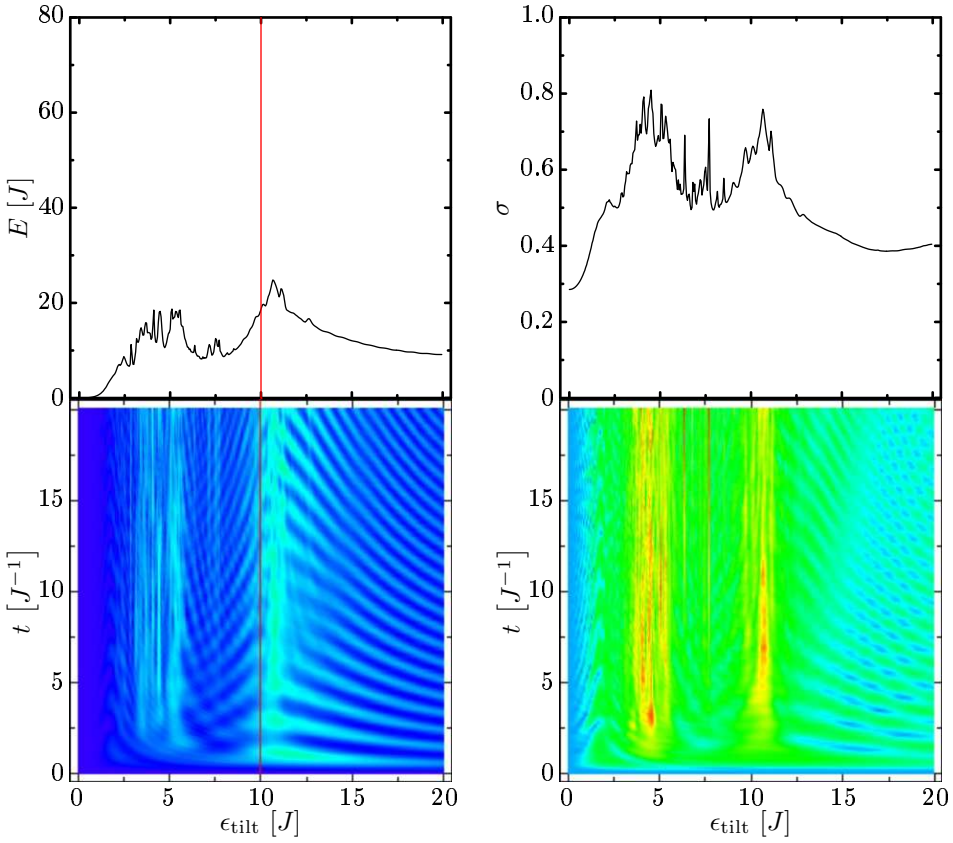

Figure 4.3: The figure illustrates a system of 6 bosons on 6 sites of a tilted lattice at the ratio $U/J = 10$. On the left hand side the energy transfer is depicted, on the right the number variance is shown. The lower images show these observables as function of time (vertical axis) and external potential ϵ_{tilt} (horizontal axis), i.e. the potential difference between neighbouring sites. The images on top of the density plots show the time-averaged data. The red line in the energy transfer plots denotes the tilting $\epsilon_{\text{tilt}} = U$.

4.2 Modulated Lattice Potential

In this section, the simulations of various configurations of bosonic gases in amplitude modulated optical lattices. As shown in section 3.2.3, the amplitude modulation of the lattice potential provides an energy $\Delta E = \omega_{\mathrm{mod}}$ with ω_{mod} the modulation frequency. By variation of this modulation frequency one can probe the many-body in the lattice, i.e., excite the system as discussed in section 3.2.1. The modulation of the lattice has to be translated to the Hubbard model, which leads, as shown in section 3.2.3, to the parameters

$$\begin{aligned} J_{\mathrm{mod}}(t) &= J_0 \exp(-F \sin(\omega_{\mathrm{mod}} t)) \\ U_{\mathrm{mod}}(t) &= U_0 (1 + F \sin(\omega_{\mathrm{mod}} t))^{1/4}. \end{aligned}$$

These are the time-dependent parameters of the Bose Hubbard Hamiltonian, with the constants J_0 (tunnelling strength) and U_0 (interaction strength) as well as the modulation amplitude F.

In order to perform a time-evolution we have to choose an initial state. This state is obtained by exact diagonalisation of the initial Hamilton matrix at the time $t = 0$ for a given ratio U_0/J_0. This means, the time-evolution always starts with the energy eigenstate, generally the groundstate. The ratio U_0/J_0 also defines the regime in which the simulation takes place.

The results presented in this section are generated by performing time-evolutions for several modulation frequencies ω_{mod}. The response of the system during the time-evolution is measured via the energy transfer and the number variance.

We study a system of six bosons on six sites of an amplitude modulated optical lattice. The lattice has cyclic boundary conditions, i.e., particles at the first site may hop to the last site and vice versa. By these conditions one avoids boundary effects. First, we look at a system with the interaction strength $U_0 = 20\ J_0$: we compute time evolutions for modulation frequencies in the range $\omega_{\mathrm{mod}} = (0 - 40) J_0$ in steps of $\Delta\omega_{\mathrm{mod}} = 0.1 J_0$ and evaluated the observables at each timestep. Figure 4.4 shows the energy transfer, which is given by the energy expectation value evaluated with the time-evolved state $\left|\psi, t\right\rangle$ via

$$E = \left\langle \psi, t \right| \hat{\mathrm{H}}_0 \left| \psi, t \right\rangle - E_0$$

with E_0 the energy of the initial state and the initial Hamilton operator $\hat{\mathrm{H}}_0 = \hat{\mathrm{H}}(t = 0)$. Shown is the full data as function of time and modulation

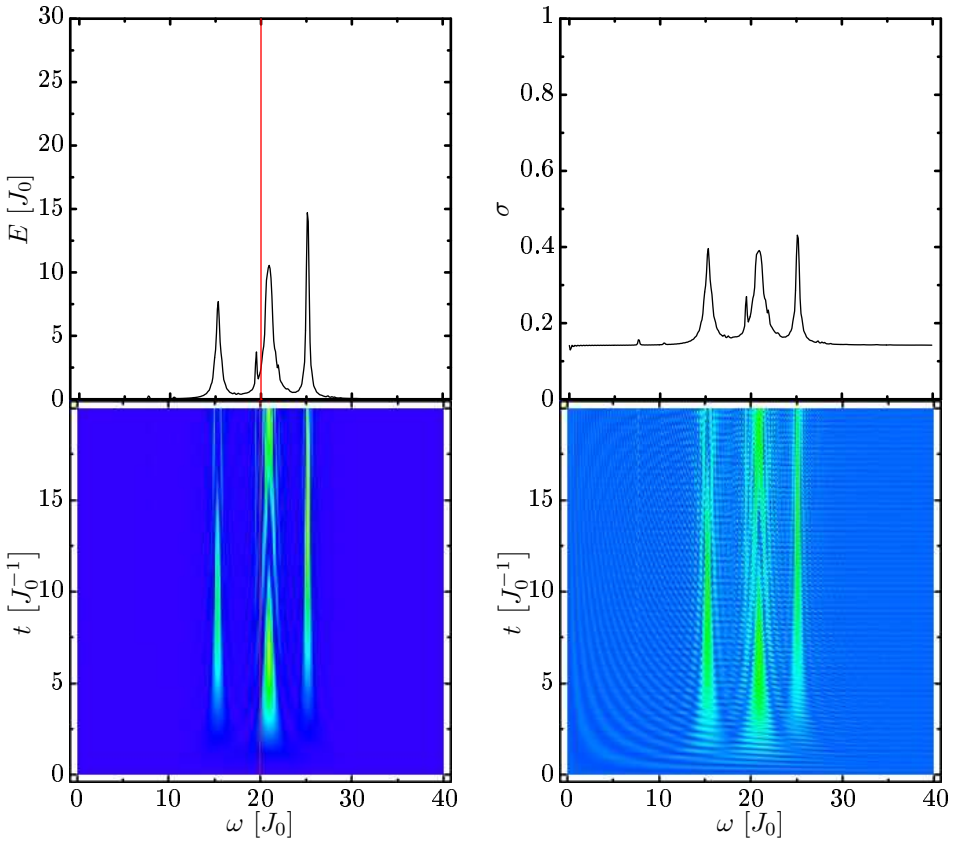

Figure 4.4: The lower density plot on the left hand side shows the energy transfer as function of time t (vertical axis) and modulation frequency ω; the plot above shows the energy transfer – averaged over time – vs. modulation frequency ω. The vertical red line denotes the energy $U_0 = 20\ J_0$, at which one would expect the main resonance in the pure Mott case. The images on the right show the number variance.

frequency and the time averaged energy transfer. One observers a triple of resonances; this triple seems to be a signature of systems with 6 bosons on 6 sites. A resonance nearby the modulation frequency $\omega_{\text{mod}} = U_0$ can be explained by a particle-hole excitation of the groundstate, which consists mainly of the Fock state $\left|1,1,1,1,1,1\right\rangle$ in the Mott regime. As discussed in section 3.2.1 one has to provide the energy U_0 to put one atom onto another in this Fock state. This energy is available at a modulation frequency $\omega_{\text{mod}} = U_0$ and thus leads to the a resonance. The centroid of this triple is slightly shifted off the $\Delta E = \omega_{\text{mod}}$-line towards higher frequencies.

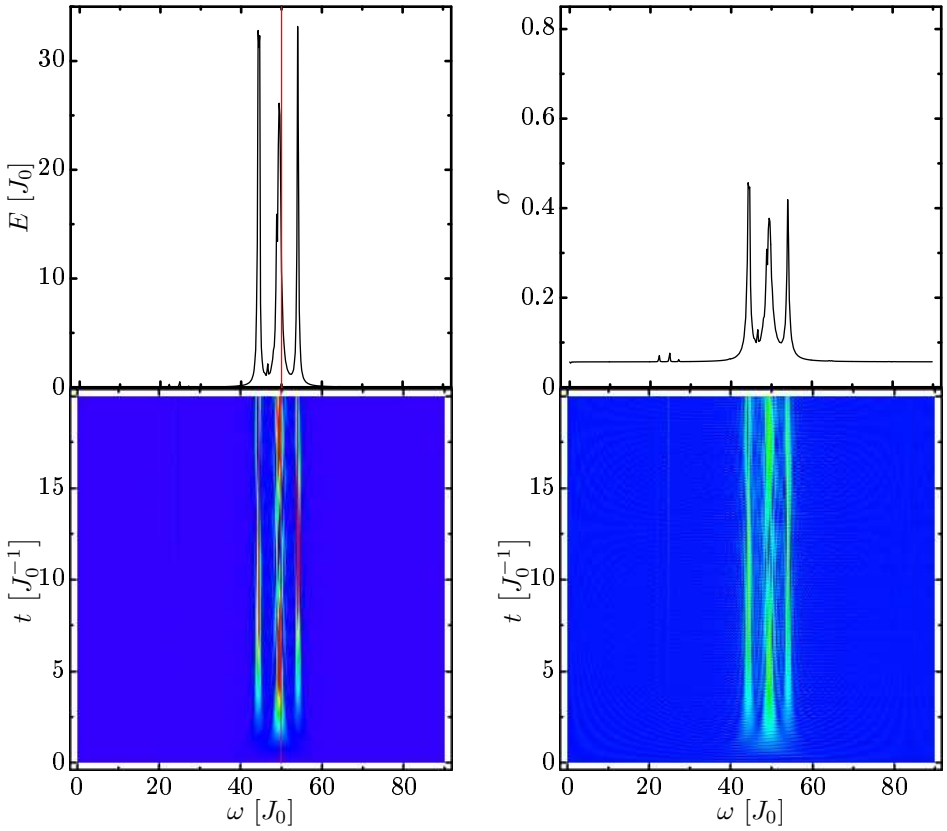

Figure 4.5: Energy transfer and the number variance of a system of 6 bosons on 6 lattice sites at a ratio $U_0/J_0 = 50$. The lower density plots show the energy transfer and number variance as function of time and modulation frequency ω_{mod}. The vertical red line denotes the frequency $\omega_{\text{mod}} = U_0/J_0$

The images on the right of Figure 4.4 show the number variance

$$\sigma_i = \langle n_i^2 \rangle - \langle n_i \rangle^2,$$

in which i is the site index. Since the lattice is translational invariant and thus the number variance is site independent, only the fluctuations at the first site are shown. The density plot on the right of figure 4.4 shows the number variance as function of time and modulation frequency, the plot above shows the time-averaged number variance. Globally, the structure is similar to the energy transfer. One observes a resonance triple and an additional, oscillatory structure in the density plot. In contrast to the energy transfer, the time averaged plot of the number variance shows a constant

background. This background is directly connected to the ratio U_0/J_0: by increasing the interaction strength U_0 (or lowering the tunnelling strength J_0) hopping will be suppressed and the number variance will disappear. In the limit of an infinite interaction strength, the system can be assumed as the *single* Fock state $|1,1,1,1,1,1\rangle$, thus, there is no variance in the occupation number. The oscillatory structure in the number variance plots is due to the oscillating strengths $J(t)$ and $U(t)$ which depend on $\sin(\omega_{\text{mod}}t)$. Plotting the values of this sine function in an array ω_{mod} versus t leads to this structure.

Figure 4.5 depict the results for a many-body system of six bosons on six lattice sites with an interaction strength $U_0 = 50\ J_0$. In contrast to the previous case, this system is deeper in the Mott regime. Again, one can see the triple-resonance structure in the energy transfer (images on the left figure 4.5) as well as in the number variance (images on the right of figure 4.5). In the time-averaged plot of the number variance one can see an additional resonance near a modulation frequency $\omega_{\text{mod}} \approx U_0/2 = 25\ J_0$, which also shows the triple peak signature. Thus, in the further discussion we call such a bunch of peaks a resonance. In the case of system above that would be 2 resonances at $\omega_{\text{mod}} = 50$ and $\omega_{\text{mod}} = 25$, each consiting of 3 peaks. Later in this chapter we will discuss systems of different sizes and boundary conditions, which also show a different structure of resonances.

As mentioned in section 3.2.3 the excitation at $\omega_{\text{mod}} = U_0$ is induced by the absorption of a photon of this frequency. Similarly, this state can be excited by two photons of half of the energy, which results in a resonance at the modulation frequency $\omega_{\text{mod}} = U_0/2$. Accordingly, since the absorbtion of two photons is less propable the resonance is weaker.

Figures 4.6 and 4.7 show the variation of the modulation amplitude in different regimes of a system of six bosons on six lattice sites. Figure 4.6 depicts the energy transfer and figure 4.7 shows the number variance versus time and frequency. The modulation amplitude F is changed in the columns from $F = 0.01$ up to $F = 0.1$. The rows show different ratios U_0/J_0, increasing from top to bottom. By comparing the rows of figure 4.7 one can see the background of the number variance decreasing towards higher ratios U_0/J_0. The upper rows illustrate the system in the superfluid regime at $U_0/J_0 = 3$, which shows very weak excitation in comparison to the rather Mott-like systems in the second and third row. For the small modulation amplitude $F = 0.01$ the perturbation can only be seen in the number variance as

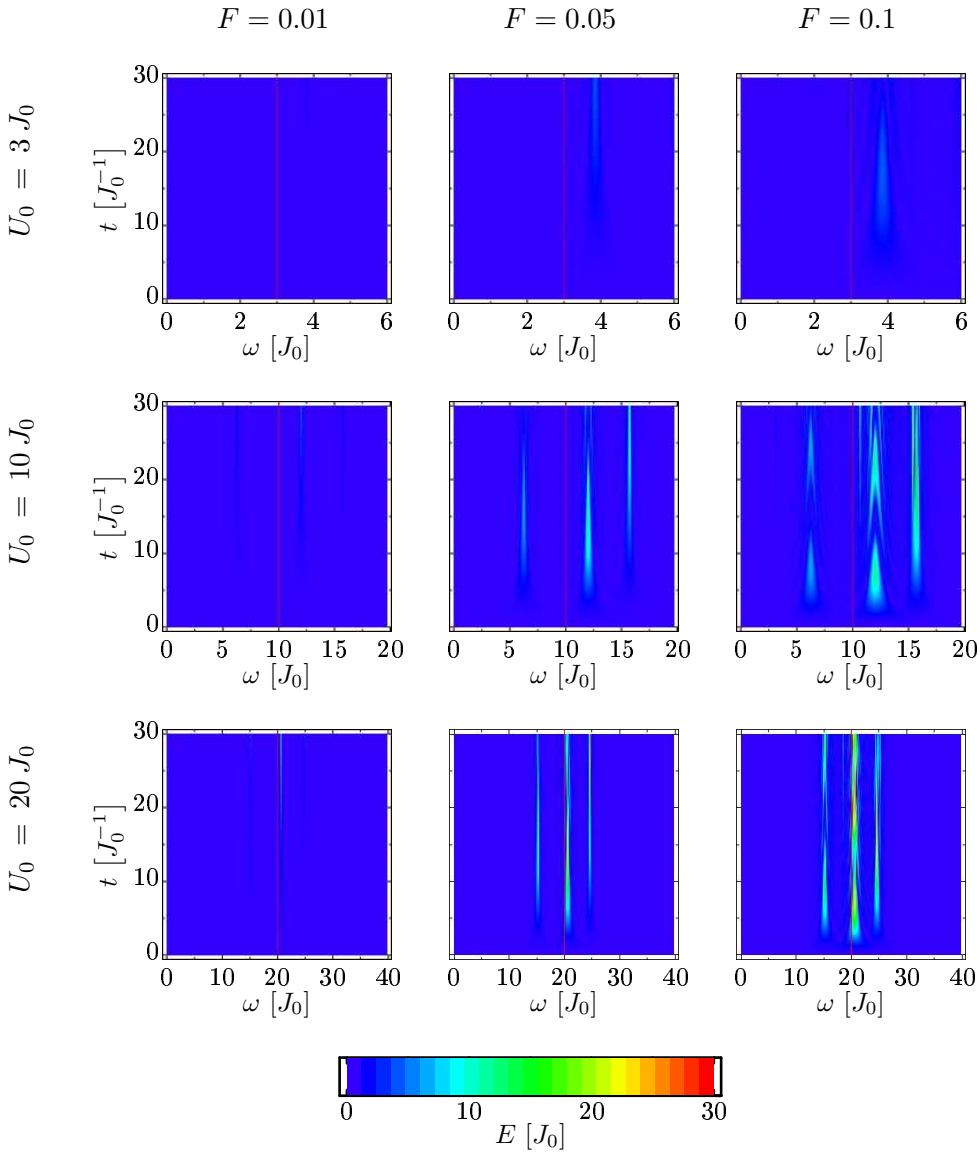

Figure 4.6: Energy transfer of a system of 6 bosons on 6 sites at different interaction strengths U_0 and modulation amplitudes $F = {}^{V_{\mathrm{mod},0}}/_{V_0}$. Each plot shows the energy transfer in the time interval $t = (0-30)\ J_0^{-1}$ vs. the modulation frequency $\omega_{\mathrm{mod}} = (0-2)\ U_0$. The rows show the interaction strengths $U_0 = 3J_0,\ 10J_0,\ 20J_0$ (top to bottom); the columns show the modulation frequencies $F = 0.01,\ 0.05,\ 0.1$.

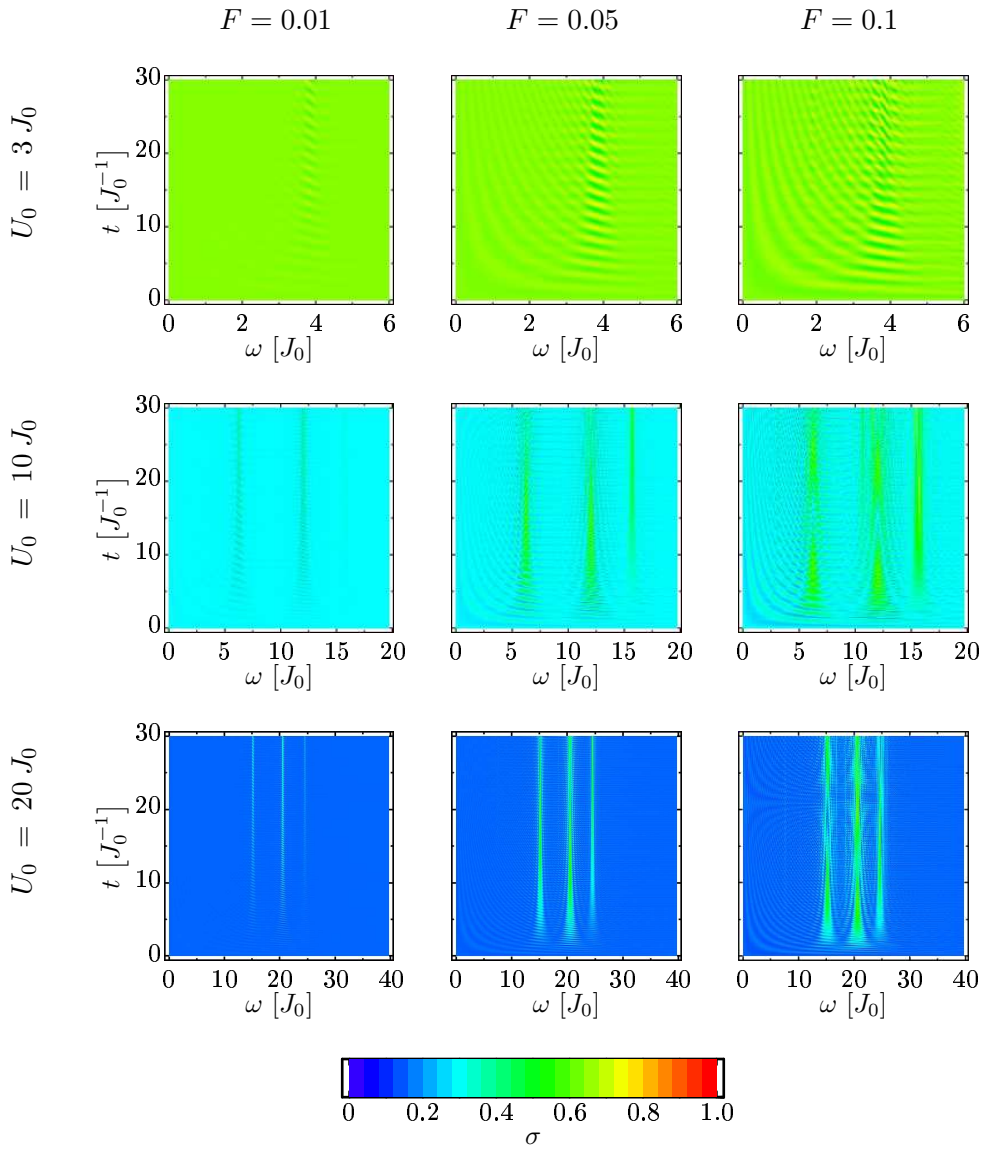

Figure 4.7: Number variance of a system of 6 bosons on 6 sites at different interaction strengths U_0 and modulation amplitudes $F = {}^{V_{\mathrm{mod},0}}/_{V_0}$. Each plot shows the number fluctuation in the time interval $t = (0 - 30)\ J_0^{-1}$ vs. the modulation frequency $\omega_{\mathrm{mod}} = (0 - 2)\ U_0$. The rows show the interaction strengths $U_0 = 3J_0,\ 10J_0,\ 20J_0$ (top to bottom); the columns show the modulation frequencies $F = 0.01,\ 0.05,\ 0.1$.

a change in the oscillatory structure at $\omega_{\mathrm{mod}} \approx 4J_0$. At stronger modulation amplitudes one observers also a weak resonance at $\omega_{\mathrm{mod}} \approx 4J_0$ appearing in the energy transfer. The second row shows the system at ${}^{U_0}/_{J_0} = 10$, which is slightly above the superfluid to Mott insulator phase transition. One can see the triple peak signature again, clearly visible in the energy transfer as well as in the number variance for modulation amplitudes $F \geq 0.05$. The third row corresponds to a ratio ${}^{U_0}/_{J_0} = 20$, which shows clear signs of resonances in the number variance already at small modulation amplitudes in the number variance.

By comparing the central peaks at different ratios ${}^{U_0}/_{J_0}$ above the superfluid to Mott insulator phase transition (figures 4.6 and 4.7), one finds that the central peak *slips* onto the frequency $\omega_{\mathrm{mod}} = U_0$ when going deeper into the Mott regime. In the limit of a very large ratio ${}^{U_0}/_{J_0}$ the groundstate of this system is approximately described by the Fock state $\big|1,1,1,1,1,1\big\rangle$, which requires exactly the energy $E = U_0$ to be excited in terms of a particle-hole excitation (section 3.2.1). By decreasing the ratio ${}^{U_0}/_{J_0}$ towards the phase transition this energy is increased due to admixtures of additional number states.

In order to analyse the excitation mechanisms in the case of a modulated lattice we have a more detailed look at the resonances. In the Mott regime, the dominant Fock state is, assuming a system in which the number of atoms equals the number of lattice sites,

$$\big|\psi_0\big\rangle \approx \big|1,1,1,\cdots,1\big\rangle,$$

with $\big|\psi_0\big\rangle$ denoting the groundstate. Obviously, one has to excite this state in order to transfer energy into the system. Since a state $\big|\psi,t\big\rangle$ at time t is characterised by the coefficients $c_\nu(t)$

$$\big|\psi,t\big\rangle = \sum_{\nu=1}^{D} c_\nu(t)\,\big|\{n_1,\cdots,n_I\}_\nu\big\rangle,$$

with I the number of lattice sites and D the dimension of the number basis (see section 2.2), one can analyse the excitations by tracking the coefficients during the time evolution.

Therefore, we study a system of 6 sites with 6 bosons at ${}^{U_0}/_{J_0} = 20$. In contrast to the previous calculations, we consider only the three main peaks (see figure 4.8, left hand side), and perform time-evolutions at the

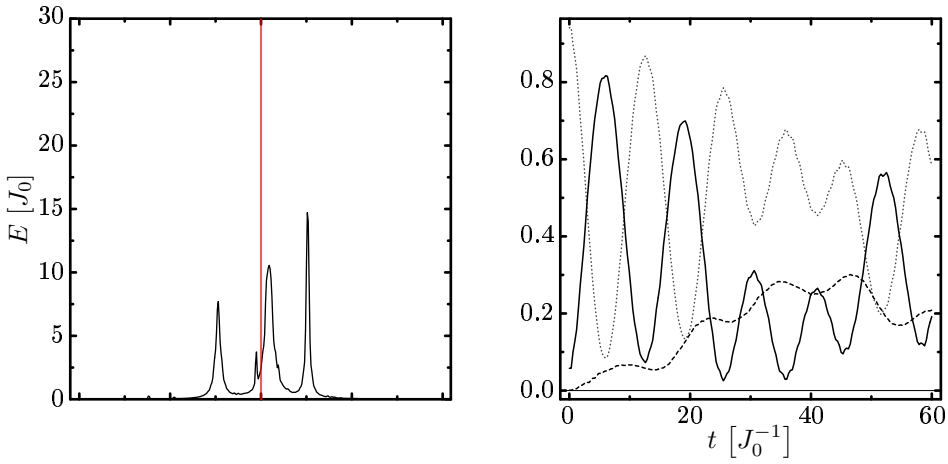

Figure 4.8: Left hand sides plot shows the average energy transfer. The plot on the right depicts the time evolution of contribution of the state $|\psi, t\rangle$ at the modulation frequency $\omega_{\text{mod}} = 20.8 J_0$: The dotted line illustrates the evolution of the Fock state $|1,1,1,1,1,1\rangle$, the solid line shows the contribution of Fock states with one doubly occupied site, and the dashed line are states with two doubly occupied sites. One can see clearly the challenge between the state $|1,1,1,1,1,1\rangle$ and the Fock states with one doubly occupied site, which is driven by particle-hole excitations.

modulation frequencies $\omega_{\text{mod}} = 15.3\ J_0,\ 20.8\ J_0,\ 25.5\ J_0$. Instead of directly evaluating observables during the calculations, we record the coefficients of all 462 basis states for each timestep. These coefficients allow us to analyse the composition of the state $|\psi, t_n\rangle$ at each timestep t_n of the evolution, and to obtain information on the mechanisms which lead to excitation in the case of a resonance. In order to reduce the large amount of information the coefficients provide, we classified the Fock states according to the distribution of the occupation numbers. For example, all states with exactly one doubly occupied site represent a class, all states with two doubly occupied sites constitute another, and so on. In terms of this classification scheme one can sum up the square of the magnitude of the coefficients $|c_i|^2$ (since $|c_i|^2$ is the propability of the i-th Fock state) corresponding to a certain class for each timestep.

Figures 4.8 and 4.9 show the results of these calculations. The plot on the left hand side of figure 4.8 depicts the time-averaged energy transfer for comparison. The plot on the right hand side of figure 4.8 illustrates the contributions to the central peak: the dotted line shows the square of the magnitude of the coefficient of the state $|1,1,1,1,1,1\rangle$, which is assumed

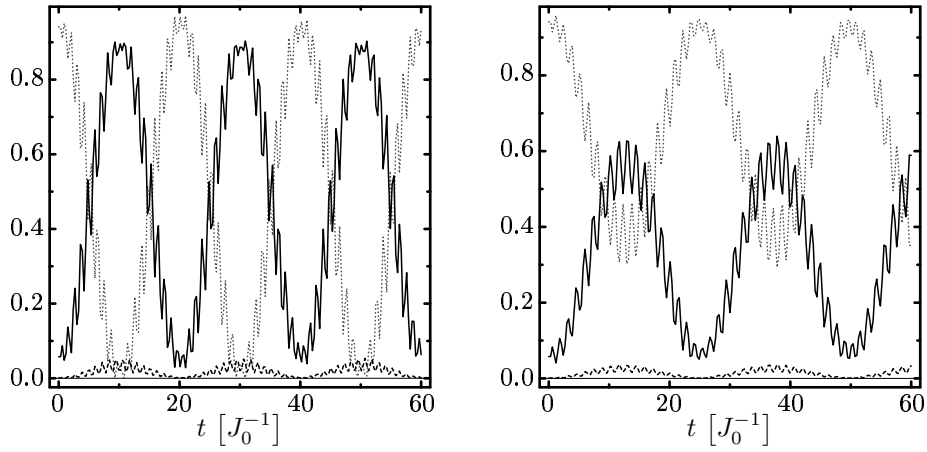

Figure 4.9: Left hand sides plot shows the composition of the system state of the peak at $\omega_{\mathrm{mod}} = 15.3\ J_0$, and the plot on the right at $\omega_{\mathrm{mod}} = 25.5\ J_0$. The dotted line is the coefficient of the Fock state $|1,1,1,1,1,1\rangle$, the solid line shows the contribution of all states with exactly on doubly occupied site, and the dashed line are states with two doubly occupied sites.

to be dominantly occupied in the Mott regime. The solid line shows the contribution of Fock states with exactly one doubly occupied site. One can see, that a decrease of the coefficient for the Fock state $|1,1,1,1,1,1\rangle$ leads to an increase of the coefficients of the states with doubly occupied sites, and vice versa. Moreover, Fock states with two doubly occupied sites also contribute to the state. These Fock states are not directly populated from of the state $|1,1,1,1,1,1\rangle$, since this excitation would require the energy $\Delta E \approx 2U_0$. These states are more likely populated via particle-hole excitations of states with one doubly occupied site, which would also explain the delayed increase of the coefficients visible in figure 4.8.

Figure 4.9 illustrates the evolution of the summed coefficients at the modulation frequencies $\omega_{\mathrm{mod}} = 15.3\ J_0$ (left hand side) and $\omega_{\mathrm{mod}} = 25.5\ J_0$ (plot on the right). In both cases one can see the same behaviour as for the central peak: the Fock states with one doubly occupied site are populated at the expense of the Fock state $|1,1,1,1,1,1\rangle$. One can also see the population of Fock states with two doubly occupied sites, but their coefficient is smaller as in the case of the central resonance peak. In contrast to the central peak, one observers an oscillation of the coefficients with a larger frequency.

In order to get an impression of the excitations mechanisms we have a closer look at the Fock states with one doubly occupied site. These Fock

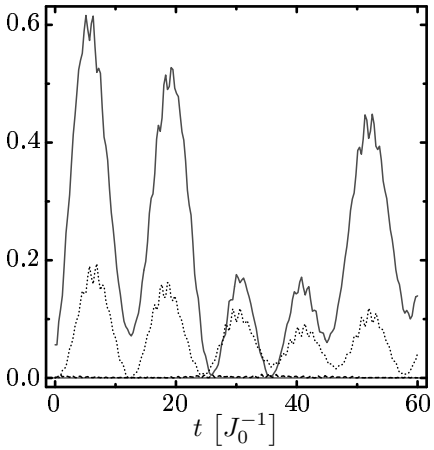

Figure 4.10: The graph depicts the coefficients of Fock states with exactly one doubly occupied site. The solid line shows the contribution of direct particle-hole excited states of $|1,1,1,1,1,1\rangle$, the other two represent states connected to $|1,1,1,1,1,1\rangle$ via one (dashed line) and two (dotted line) additional hops.

states can again be subdivided into different classes, since they include states which are directly connected to the pure Mott state $|1,1,1,1,1,1\rangle$ via a hop to a neighbouring site (particle-hole excitation), e.g.

$$\hat{a}_1^\dagger \hat{a}_2 \,|1,1,1,1,1,1\rangle = \sqrt{2}\,|2,0,1,1,1,1\rangle.$$

Directly connected means, that the matrix element of the Hamiltonian between these two states is non-vanishing. Therefore, the particle-hole excited states are classified by the distance between the doubly occupied and non-occupied site. All Fock states with the distance $d = 0$ (the doubly and non-occupied site are direct neighbours) are directly connected to the pure Mott state $|1,1,1,1,1,1\rangle$, $d = 1$-states are connected to $d = 0$ states via a hop, and so on. In the further discussion, we leave out the '='-sign and use dn-state as a abbreviation for all states, which are connected by n hops to a $d = 0$-state:

$$\underbrace{|2,\overset{\curvearrowleft}{0},1,1,1,1\rangle}_{d0\text{-state}} \longrightarrow \underbrace{|2,1,\overset{\curvearrowleft}{0},1,1,1\rangle}_{d1\text{-state}} \longrightarrow \underbrace{|2,1,1,0,1,1\rangle}_{d2\text{-state}}.$$

Figure 4.10 illustrates the evolution of the coefficients of Fock states directly connected to $|1,1,1,1,1,1\rangle$ (solid line), and Fock states which are connected to this state via an particle-hole excitation and one (dotted line) or two (dashed line) hops. The $d0$-states are mainly occupied, since they benefit from the direct connection to the Fock state $|1,1,1,1,1,1\rangle$. Interestingly, $d1$-states, which are connected to $|1,1,1,1,1,1\rangle$ by an additional hop are almost not occupied in comparison to $d2$-states.

Figure 4.11 shows the same situation in the case of the peaks at $\omega_{\mathrm{mod}} = 15.3\ J_0$ (left hand side) and $\omega_{\mathrm{mod}} = 25.5\ J_0$ (right hand side). In compar-

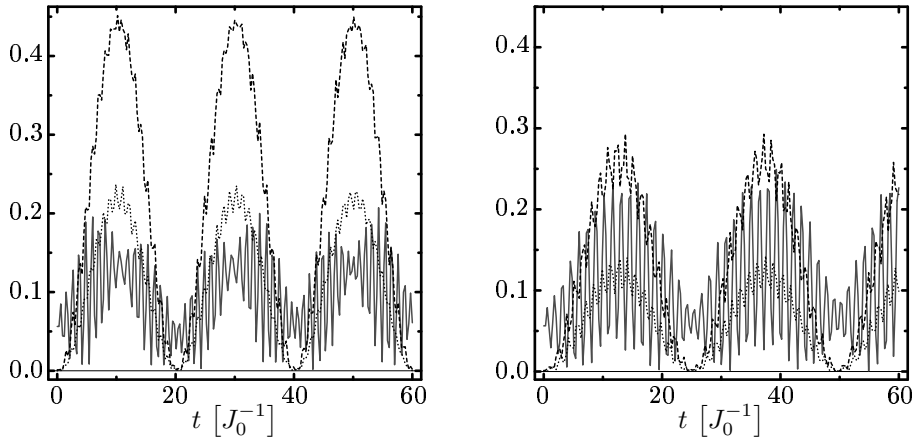

Figure 4.11: The graph depicts the coefficients of Fock states with exactly one doubly occupied site on the peaks at $\omega_{\mathrm{mod}} = 15.3\ J_0$ (left) and $\omega_{\mathrm{mod}} = 25.5\ J_0$ (right). The solid line shows the contribution of direct particle-hole excited states of $|1,1,1,1,1,1\rangle$, the other two represent states connected to $|1,1,1,1,1,1\rangle$ via one (dashed line) and two (dotted line) additional hops.

ison to the central resonance peak the Fock states which are not directly connected to the pure Mott state are much stronger: In the case of the resonance peak, at $\omega_{\mathrm{mod}} = 15.3\ J_0$ the $d1$-states are populated dominantly. The particle-hole excited $d0$-states themselfes show a superposed oscillation with a rather high frequency in both peaks, $\omega_{\mathrm{mod}} = 15.3\ J_0$ and $\omega_{\mathrm{mod}} = 25.5\ J_0$.

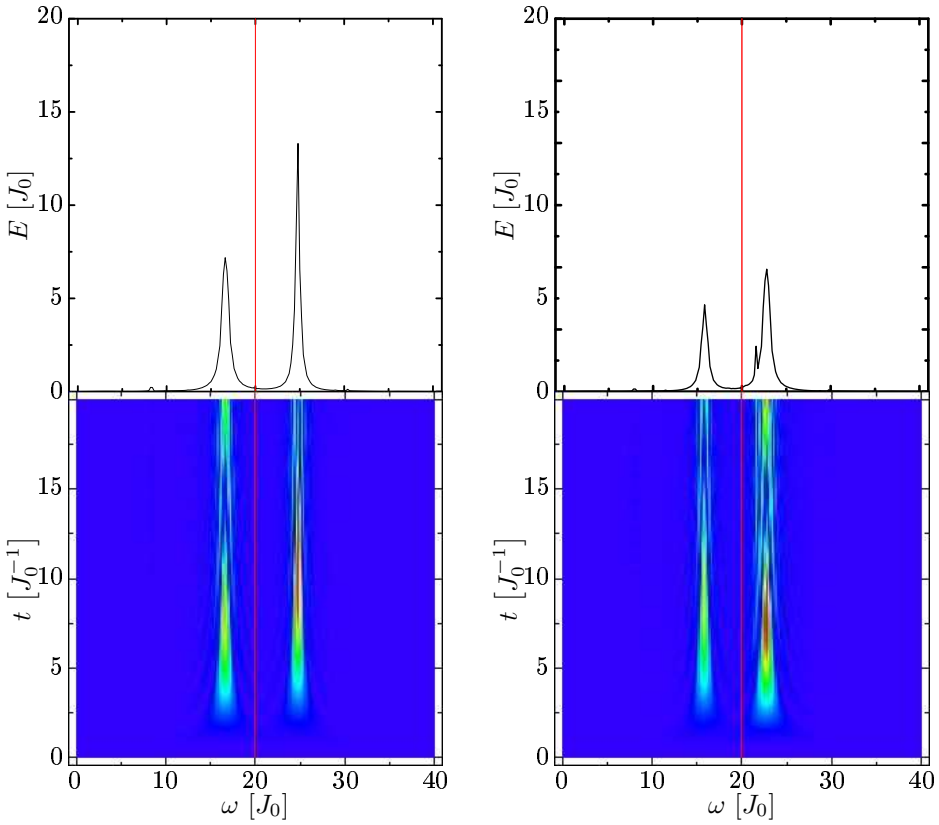

Figure 4.12: Energy transfer of a system of 4 bosons on 4 lattice sites (left) and 5 bosons on 5 lattice sites, both at a ratio $U_0/J_0 = 20$. Shown is the energy transfer as function of time and modulation frequency ω_{mod} (lower images) and the time-averaged values (upper images). In both cases one can see a 2-peak signature.

We assume the structure of the resonances to be an effect of the finite size of the lattices. Therefore, we varied the number of atoms and sites in the following simulations. Figure 4.12 illustrates the energy transfer of systems of 4 (left hand side) and 5 (right hand side) sites, both with an average filling factor of 1 boson per site. Both simulations are performed at the ratio $U_0/J_0 = 20$. The density plots show the energy transfer as function of time and modulation frequency ω_{mod}, the plots above depict the energy transfer, time-averaged over the whole simulation from $t = 0$ to 20 J_0^{-1}. In contrast to the 6 boson systems discussed before, these show a two-peak resonance structure. Again, the resonance frequency $\omega_{\text{mod}} = U_0$, regarding the centroid of the resonance, is in agreement with the particle-hole excitation picture.

Figure 4.13 illustrates the energy transfer of 7 bosons on 7 sites (left hand

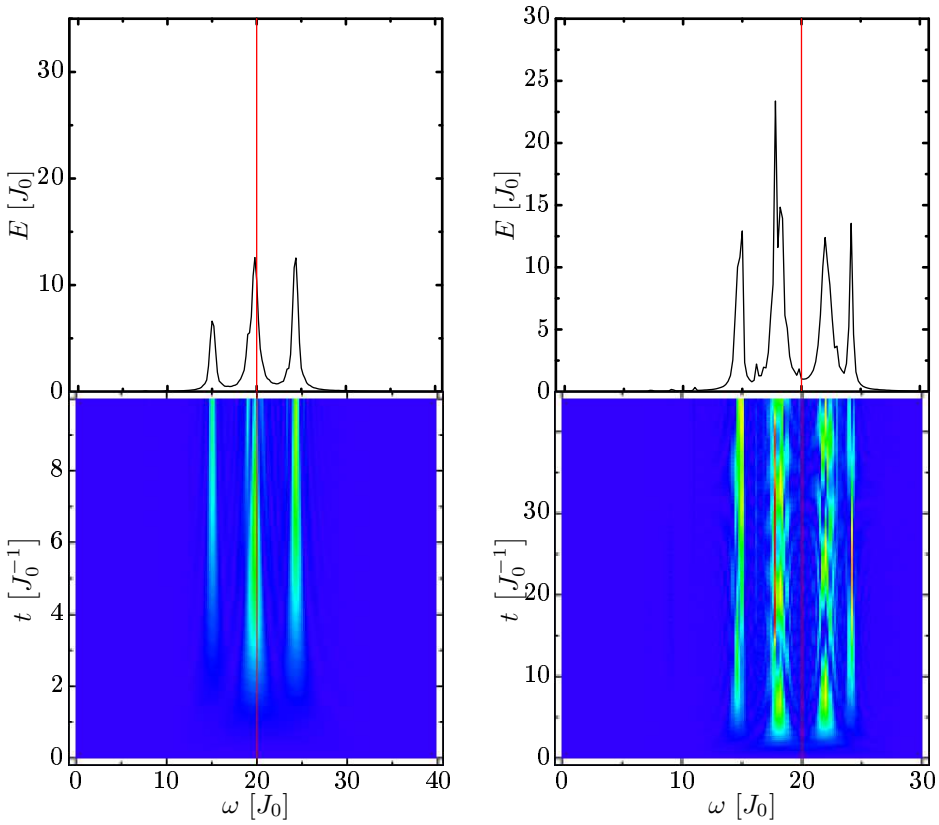

Figure 4.13: Energy transfer of a system of 7 bosons on 7 lattice sites (left) and 8 bosons on 8 lattice sites, both at a ratio $U_0/J_0 = 20$. Shown is the energy transfer as function of time and modulation frequency ω_{mod} (lower images) and the time-averaged values (upper images). The 7 boson system shows a 3-peak signature similar to the 6 boson-6 sites system; the 8 boson-8 sites system shows a 4 peak resonance structure.

side) and 8 bosons on 8 sites (right hand side) at the ratio $U_0/J_0 = 20$. The 7-boson system shows a similar resonance structure as the 6-boson system; again the centroid of the triple peak is close to the frequency $\omega_{\mathrm{mod}} = U_0$ as proposed by the particle-hole excitation picture. The same holds true for the 8 boson system, although the resonance consists of 4 peaks, whose centroid is also close to the frequency $\omega_{\mathrm{mod}} = U_0$.

Figure 4.14 shows a lattice of 5 sites with 10 bosons at $U_0/J_0 = 20$, which shows a rich excitation spectrum: The strongest peak appearing in the energy transfer at $\omega_{\mathrm{mod}} = U_0$ (left hand side of figure 4.14) represents the particle-hole excitations of the pure Mott-state to $d0$-states. Left of it one can see a resonance at $U_0/2$, which indicates the absorbtion of two photons

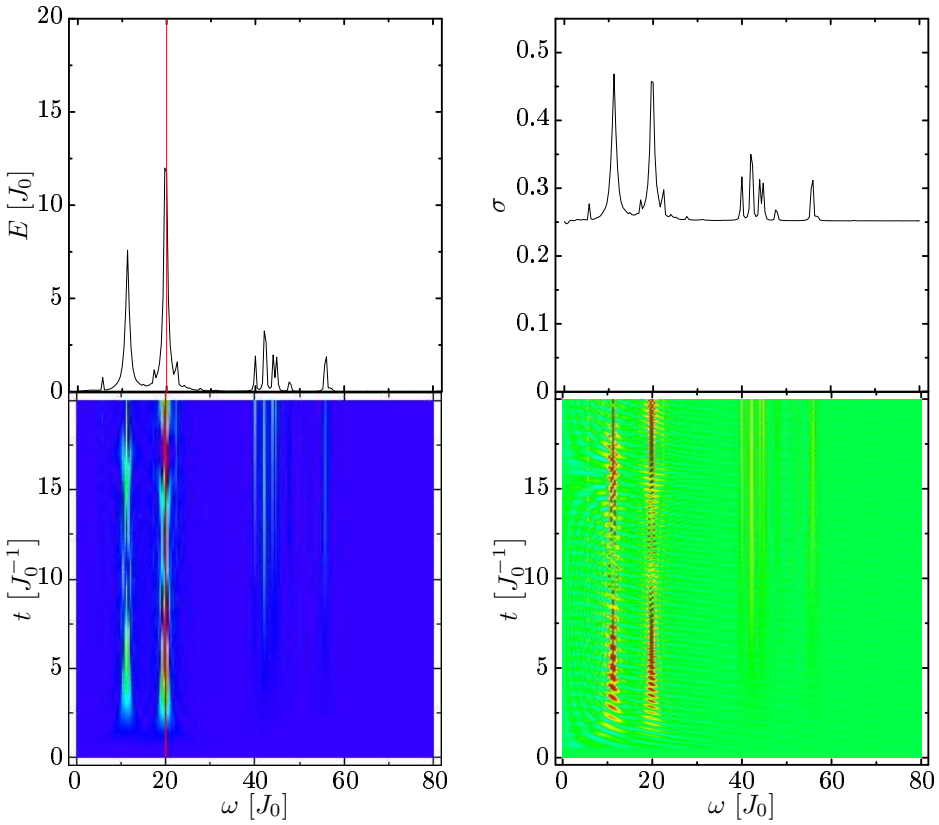

Figure 4.14: Energy transfer (left hand side) and number variance (right hand side) of 10 bosons on 5 lattice sites with a ratio $U_0/J_0 = 20$. The density plots depict the observables as function of time and modulation frequency ω_{mod}, the plots on top illustrate these values averaged over time $t = (0-20)\ J_0$. The red line in the energy transfer plots denote the frequency $\omega_{\mathrm{mod}} = U_0/J_0$. This system shows resonances nearby the frequencies $\omega_{\mathrm{mod}} = U_0,\ 2U_0,\ \sim 3U_0$.

of the energy $E = U_0/2$, which also leads to the excitation of the pure Mott state. The tiny peak at $U_0/3$ indicates a three photon absorbtion, each of the energy $E = U_0/3$. Additionally, resonances appear at integer multiples of U_0: the multi-peak structure at $\omega_{\mathrm{mod}} = 2U_0$ is generated by two parallel particle-hole excitations of the pure Mott state with a photon of the energy $E = 2U_0$. The resonance at $\sim 3U_0$ indicates 3 parallel particle-hole excitations. The propability of these excitations is reduced in comparision to the resonances at $\omega_{\mathrm{mod}} = U_0$ and $\omega_{\mathrm{mod}} = U_0/2$, since the Hamiltonian does not connect the pure Mott state $\left|2,2,2,2,2\right\rangle$ with a state $\left|3,3,1,1,2\right\rangle$.

Figure 4.15 shows the simulation of a system of 7 bosons on 6 lattice sites at the ratio $U_0/J_0 = 20$. In contrast to the parameter sets discussed

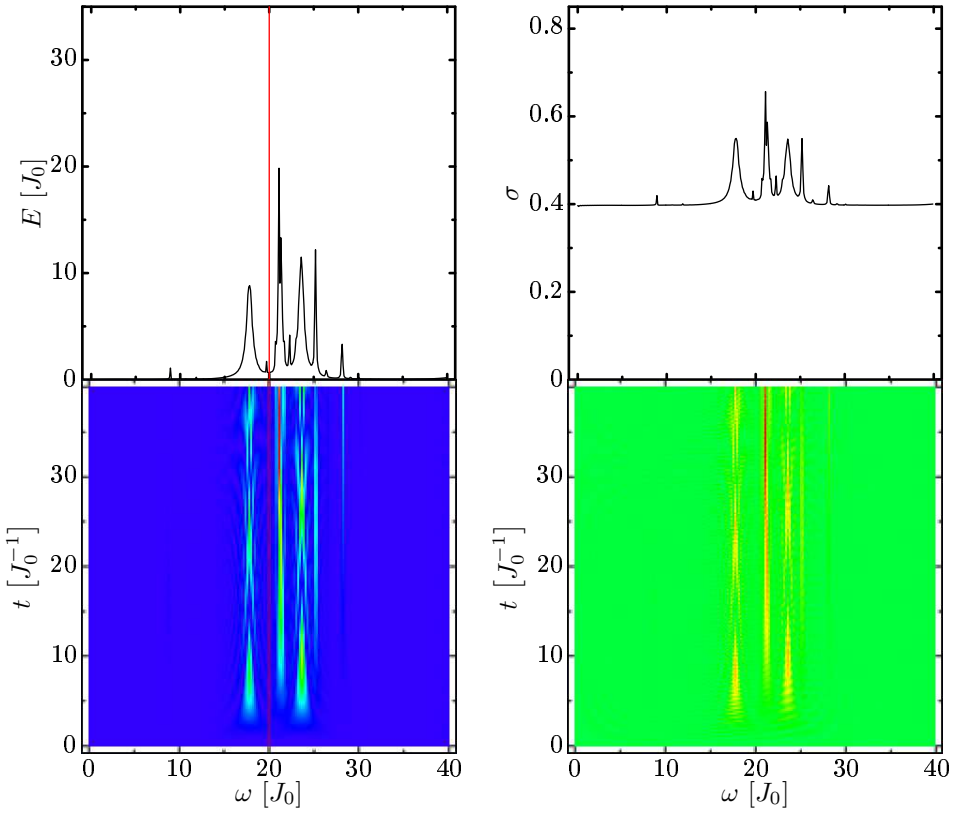

Figure 4.15: Energy transfer (left hand side) and number variance (right hand side) of 7 bosons on 6 lattice sites with an ratio $^{U_0}/_{J_0} = 20$. The density plots depict the observables as function of time and modulation frequency ω_{mod}, the plots on top illustrate these values averaged over time $t = (0 - 40)\ J_0$. The red line in the energy transfer plots denote the frequency $\omega_{\mathrm{mod}} = {}^{U_0}/_{J_0}$.

earlier in this chapter, this system has a non-commensurate filling factor. This results in a stronger background in the number variance (right hand side of figure 4.15) even at large $^{U_0}/_{J_0}$. Six of the seven bosons would form a Mott insulating state as discussed earlier in this chapter, but the remaining boson is delocalised over the whole lattice and generates fluctuations due to its mobility. This arrangement produces a resonance structure different from that of the systems with commensurate filling factor, which implies, that the number of peaks appearing depends on the size of the lattice as well as on the filling factor.

Finally, we simulated a 6 boson 6 site system with box-boundary conditions. The figures 4.16 ($^{U_0}/_{J_0} = 20$) and 4.17 ($^{U_0}/_{J_0} = 50$) illustrate the energy transfer and number variance of such systems. Compared to the

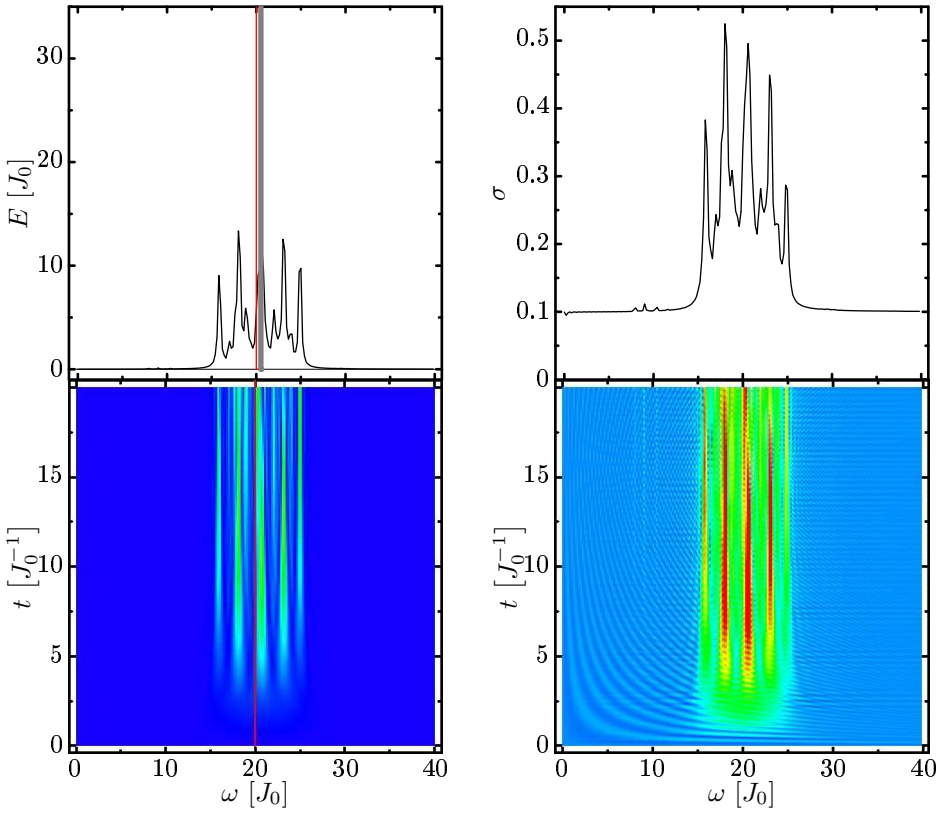

Figure 4.16: The density plot on the left shows the energy transfer of a system of 6 bosons on 6 sites of a lattice with box boundary conditions at the ratio $U_0/J_0 = 20$. The lower image shows the energy transfer plotted over modulation frequency ω_{mod} and time. The gray line in the time-averaged plot denotes the centroid of the peaks in the region $\omega_{\mathrm{mod}} \approx (15 - 25)\ J_0$. The plots on the right illustrate the number fluctuations σ at the first site; the lower plot shows the fluctuation over time and modulation frequency $\omega_{\mathrm{mod}} \approx (15{-}25)\ J_0$, the graph above shows the time-averaged fluctuations.

cyclic boundary conditions two more peaks appear in the resonance structure, but the resonance frequency is again in good agreement with the prediction of the particle-hole excitation picture. In comparison with the same system with cyclic boundary conditions, the width of the resonance structure stays the same. In both cases, the distance between the two outer peaks is $\Delta\omega_{\mathrm{mod}} \approx 10\ J_0$. Both non-cyclic systems show also a weak resonance structure at the frequency $\omega_{\mathrm{mod}} = U_0/2$.

The simulation illustrated in figure 4.18 is again a system of 6 bosons on 6 lattice sites with box boundary conditions and an superposed harmonic

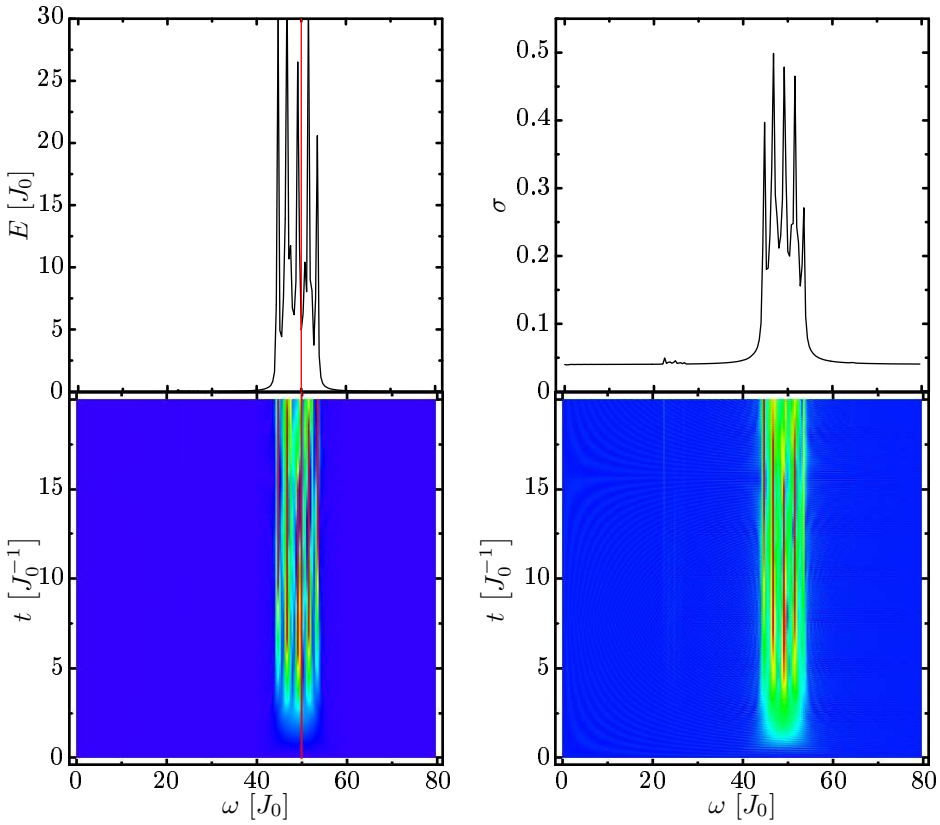

Figure 4.17: Energy transfer (left hand side) and number variance (right hand side) of 6 bosons on 6 lattice sites with a ratio $U_0/J_0 = 50$ and box boundary conditions. The density plots depict the observables as function of time and modulation frequency ω_{mod}, the plots on top illustrate these values averaged over the time $t = (0 - 20)\ J_0$. The red line in the energy transfer plots denote the frequency $\omega_{\text{mod}} = U_0/J_0$.

trapping potential, which resembles the actual experimental setups. This external potential is introduced through the on-site energy ϵ_i of the Bose Hubbard Hamiltonian. In case of a harmonic trapping potential these parameters read

$$\epsilon_i = 4V_{\text{trap},0}\left(\frac{i}{I} - \frac{1}{2}\right)^2 \tag{4.2}$$

with I the number of lattice sites and $V_{\text{trap},0}$ the trapping potential at the outer sites. This harmonic trap is symmetric with respect to the centre of the lattice, where the potential vanishes. The spectrum is similar to the system without a harmonic trapping potential, it shows a resonance for the modulation frequency $\omega_{\text{mod}} = U_0$ and an additional weak resonance at

$\omega_{\mathrm{mod}} = 3U_0$.

In conlusion, for the modulated lattice one can say that the resonance frequencies motivated by the particle-hole excitation picture are in good agreement with the resonances obtained in the simulation. Nevertheless, we cannot explain the fine structure of these resonances, which depend on the size of the lattice as well as on the number of atoms and boundary conditions.

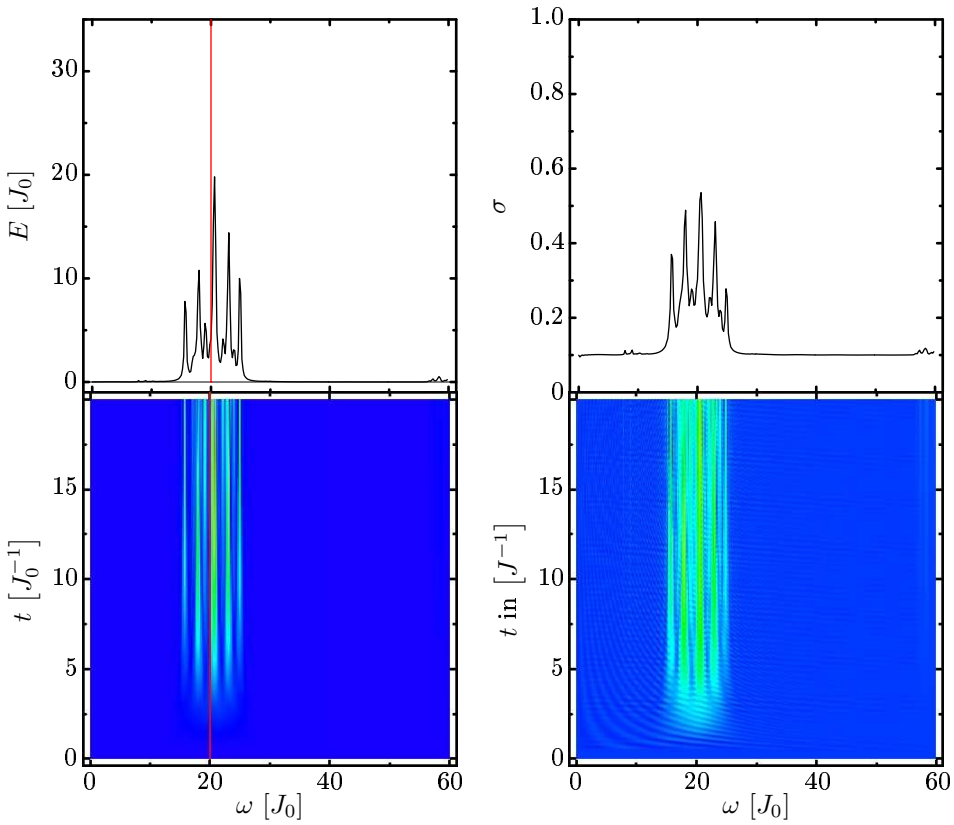

Figure 4.18: Six bosonic atoms on six sites of an amplitude modulated lattice with non-cyclic boundary conditions and a parabolic trapping potential, at an interaction strength $U_0 = 20$ and tunnelling strength $J_0 = 1$. Depicted is the energy transfer (left hand side) and the number fluctuations (right hand side). The density plots show the observables as function of time and modulation frequancy, the plots above show the values averaged over the time of the simulation. The trapping potential is $V_{\text{trap}} = U_0$ at the boundaries (sites 1 and 6) and $V_{\text{trap}} = 0$ in the centre of the lattice (between sites 3 and 4).

Chapter 5

Fermions

In this chapter the simulations of a two-component fermion gas in an optical lattice are presented. Analogously to the calculations of the Bose gases, pertubations by tilted and modulated lattices amplitudes are discussed.

5.1 Tilted Lattice Potential

In this section the excitation spectrum of a two-component fermion system with 6 lattice sites is probed by lattice tilting. Each of the two fermionic species contributes 3 atoms. Analogous to the discussion for a bosonic systemin section 3.2.2 , the Fermi Hubbard Hamiltonian (2.55) can be extended in the same way: by introducing an additional on-site energy term

$$\begin{aligned}\hat{\mathrm{H}}_{\mathrm{FF}} = &-J\sum_{i=1}^{I}\left(\hat{\mathrm{c}}_i^{\dagger}\hat{\mathrm{c}}_{i+1}+\hat{\mathrm{c}}_{i+1}^{\dagger}\hat{\mathrm{c}}_i\right)-J\sum_{i=1}^{I}\left(\hat{\mathrm{d}}_i^{\dagger}\hat{\mathrm{d}}_{i+1}+\hat{\mathrm{d}}_{i+1}^{\dagger}\hat{\mathrm{d}}_i\right)\\ &+U_{\mathrm{cd}}\sum_{i=0}^{I}\hat{\mathrm{n}}_i^{(c)}\hat{\mathrm{n}}_i^{(d)}+\sum_{i=0}^{I}\epsilon_i\left(\hat{\mathrm{n}}_i^{(c)}+\hat{\mathrm{n}}_i^{(d)}\right).\end{aligned}$$

Generally, each species would have its own on-site energy term. In our case, this external potential is assumed to be the same for both kinds of fermions. The parameter ϵ_i is defined by

$$\epsilon_i = i\epsilon_{\mathrm{tilt}},$$

with ϵ_{tilt} the site-independent energy difference between neighbouring sites and i the site index. The excitation spectrum is probed by variation of the

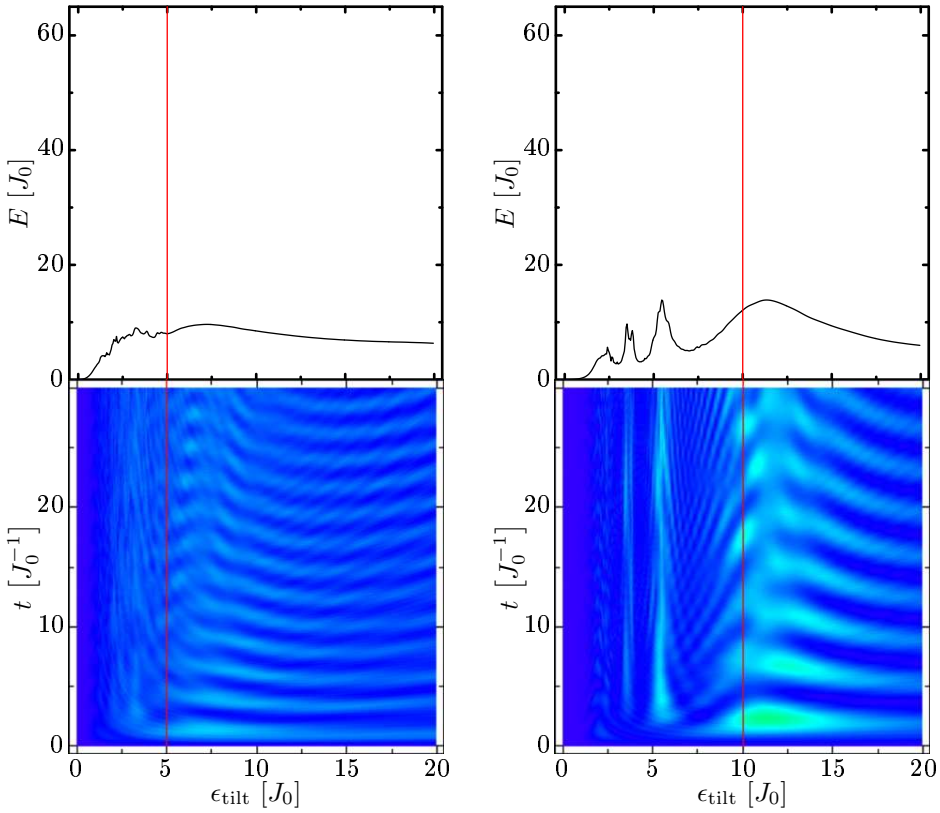

Figure 5.1: Energy transfer of a system of two fermionic species on 6 lattice sites. Each species contributes 3 atoms. Left hand side shows the system at the ratio $U_{\text{cd}}/J = 5$, right hand side at $U_{\text{cd}}/J = 10$. Depicted is the energy transfer as function of time and lattice tilting ϵ_{tilt} (density plots in the lower row) and the time-averaged energy transfer over the whole simulation. The red line denotes the tilting ϵ_{tilt} which corresponds to the interaction strength U_{cd}.

lattice tilting ϵ_{tilt}. In the strongly repulsive regime, the groundstate does not contain Fock states with doubly occupied sites. If the energy difference between sites overcomes the interaction energy due to the tilt, the system responds with a particle-hole excitation. One has to keep in mind, that, due to the Pauli exclusion principle, interaction occurs only between two fermion of different species.

Figures 5.1 and 5.2 illustrate the simulation of a two-component fermion system at different ratios U_{cd}/J, increasing from a weakly interacting system with $U_{\text{cd}} = 5\ J$ up to $U_{\text{cd}} = 50\ J$. In all cases the simulation starts with the groundstate corresponding to the ratio U_{cd}/J at the time $t = 0$ with the non-tilted Hamiltonian. At time $t = 0.1\ J$ the tilt is immediately applied

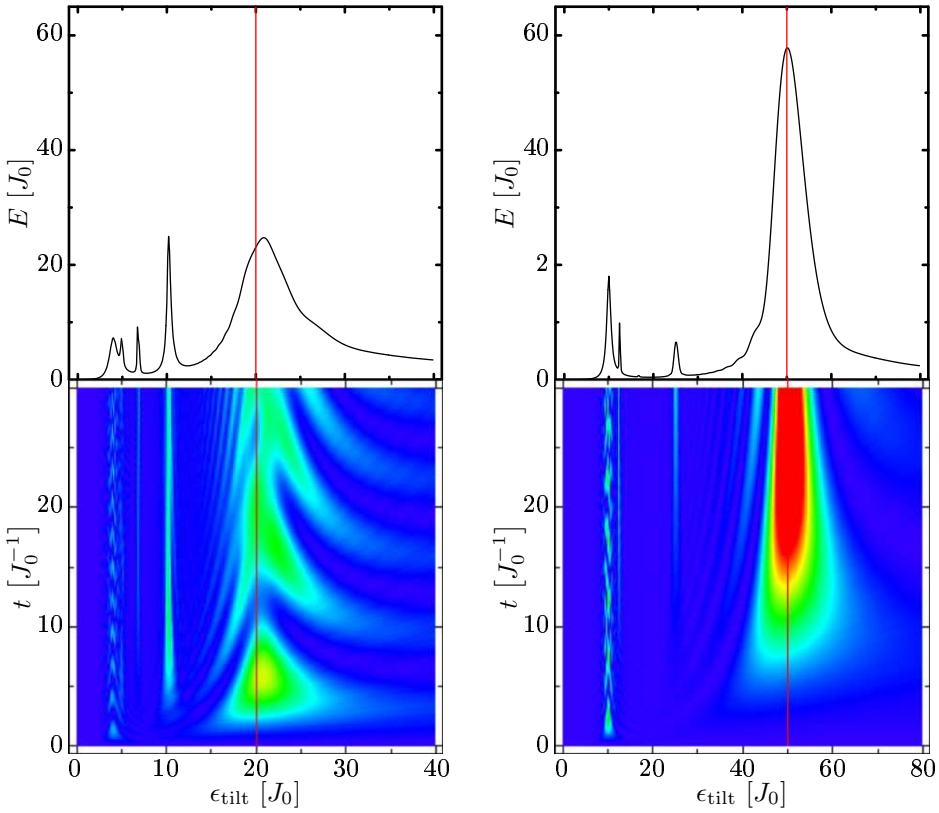

Figure 5.2: Energy transfer of a system of two fermionic species on 6 lattice sites. Each species contributes 3 atoms. Left hand side shows the system at the ratio $U_{\text{cd}}/J = 20$, right hand side at $U_{\text{cd}}/J = 50$. Depicted is the energy transfer as function of time and lattice tilting ϵ_{tilt} (density plots in the lower row) and the time-averaged energy transfer over the whole simulation. The red line denotes the tilting ϵ_{tilt} which corresponds to the interaction strength U_{cd}.

with a constant parameter ϵ_{tilt} until the simulation ends at $t = 63\ J$. The figures show the energy transfer as function of time and lattice tilt ϵ_{tilt}, and time-averaged as a function of the tilt. The time-averaging is performed over the whole time span.

The sequence of simulations illustrate the change of the excitation spectrum with the variation of the ratio U_{cd}/J. At weak interaction strengths (figure 5.1) one observes a broad and continuous spectrum, whereas in the strongly repulsive regime (figures 5.2) a discrete spectrum with sharp peaks appears.

The strongest resonance at $\epsilon_{\text{tilt}} = U_{\text{cd}}$ indicates the trivial resonance due to hopping to a neighbouring site, as discussed above. For the simulations

with ratios $^{U_{\mathrm{cd}}}/_{J} \geq 10$ peaks at fractional values of U_{cd} appear. For tilting $\epsilon_{\mathrm{tilt}} = {}^{U_{\mathrm{cd}}}/_{2}$ the energy difference between next neighbouring sites is $\Delta E = U_{\mathrm{cd}}$. In the same scheme, resonances at $\epsilon_{\mathrm{tilt}} = {}^{U_{\mathrm{cd}}}/_{3}$ and $\epsilon_{\mathrm{tilt}} = {}^{U_{\mathrm{cd}}}/_{4}$ (hopping across 4 sites) occur.

5.2 Modulated Lattice Potential

In this section the simulations of two fermionic species in an amplitude modulated lattice potential are presented. As discussed in section 2.3.2 the Fermi Hubbard Hamiltonian consits of two kinetic terms for each species. Furthermore, since fermions have to obey the Pauli exclusion principle and short-range on-site interactions are assumed, only inter-species interaction are possible. Thus, the parameters of the Fermi Hubbard Hamiltonian are the tunnelling strengths J of each species and the inter-species interaction strength U_{cd}. In this work, we restrict outselfes to a single tunnelling strength J, i.e. the parameters J of both kinetic terms are equal. The amplitude modulation of the lattice potential is implemented as it was done for the Bose Hubbard model in section 3.2.3. The time-dependent parameters of the Hamiltonian (2.55) are

$$\begin{aligned} J(t) &= J_0 \exp(-F \sin(\omega_{\mathrm{mod}} t)) \\ U_{\mathrm{cd}}(t) &= U_{\mathrm{cd}} \left(1 + F sin(\omega_{\mathrm{mod}} t)\right)^{1/4}, \end{aligned}$$

with the constant parameters J_0 and U_{cd}, the modulation frequency ω_{mod}, and the modulation amplitude F. The ratio $^{U_{\mathrm{cd}}}/_{J_0}$ controls the physics of this system, which means that for large positive ratios $^{U_{\mathrm{cd}}}/_{J_0}$ the system is in the strongly repulsive regime. Systems with commensurate filling factors, i.e. the sum of the atoms of both species equals the number of lattice sites suppresses the transport of particles in that case and form an insulating phase. On the other hand, for a dominant kinetic term $J_0 > U_{\mathrm{cd}}$ the atoms can move almost freely. In comparison to the bosons, even for an infinite strong tunnelling term the mobility is restricted due to the Pauli principle.

In order to perform a time evolution an initial state is obtained by computing the groundstate corresponding to the ratio $^{U_{\mathrm{cd}}}/_{J_0}$. The propagation is then performed using the Hamilton operator (2.55) with the time-dependent parameters given above. During this time evolution the energy transfer into the system is evaluated. As discussed in section 2.3.2 the number variance

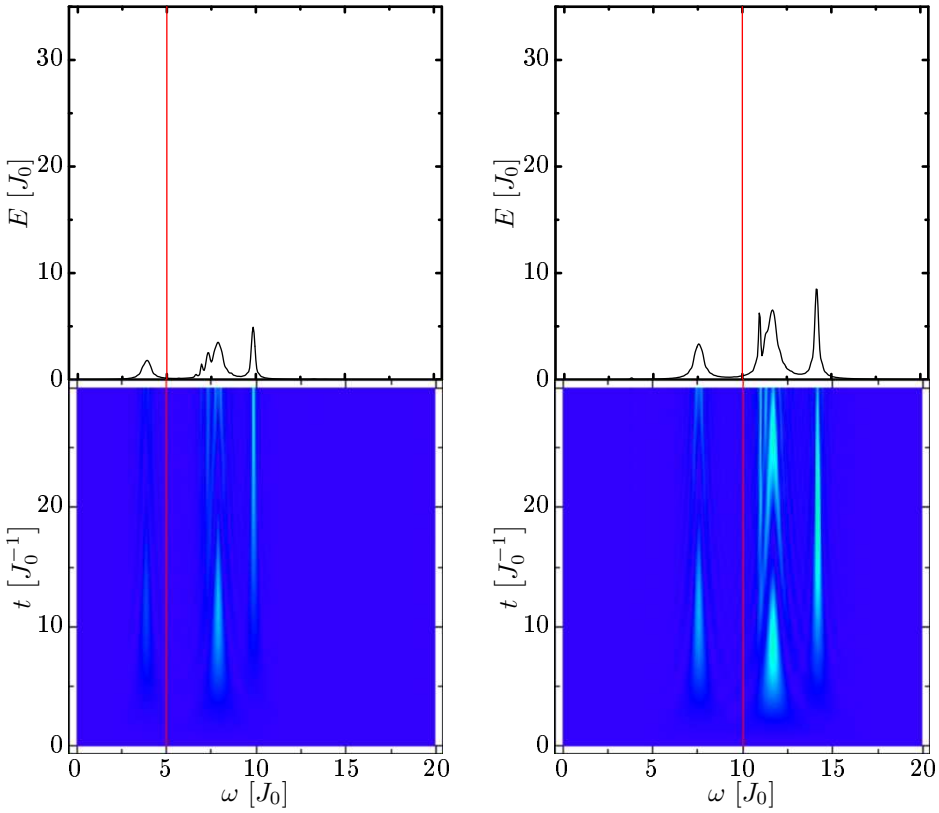

Figure 5.3: Energy transfer of a system of two fermionic species on 6 lattice sites. Each species contributes 3 atoms. Left hand side shows the system at the ratio $U_{\mathrm{cd}}/J_0 = 5$, right hand side at $U_{\mathrm{cd}}/J_0 = 10$. Depicted is the energy transfer as function of time and modulation frequency ω_{mod} (density plots in the lower row) and the time-averaged energy transfer over the whole simulation. The red line denotes the resonance frequency $\omega_{\mathrm{mod}} = U_{\mathrm{cd}}$.

σ does not reveal much information for fermionic systems due to the Pauli principle (discussed in section 2.3.3).

We have computed the time evolution of a system of 6 lattice sites with 6 fermions, 3 atoms of each species. The figures 5.3 and 5.4 illustrate the energy transfer during the time evolution of these arrangements at the ratios $U_{\mathrm{cd}}/J_0 = 5,\ 10,\ 20,$ and 50.

The fermions show a similar behaviour as the bosons in the previous chapter. The picture of particle-hole excitations predicts a resonance at the modulation frequency $\omega_{\mathrm{mod}} = U_{\mathrm{cd}}$, which is the energy needed to place one atom of each species on the same site. Similar to the bosonic systems, the multi-peak structure of the resonances seems not to be explainable by

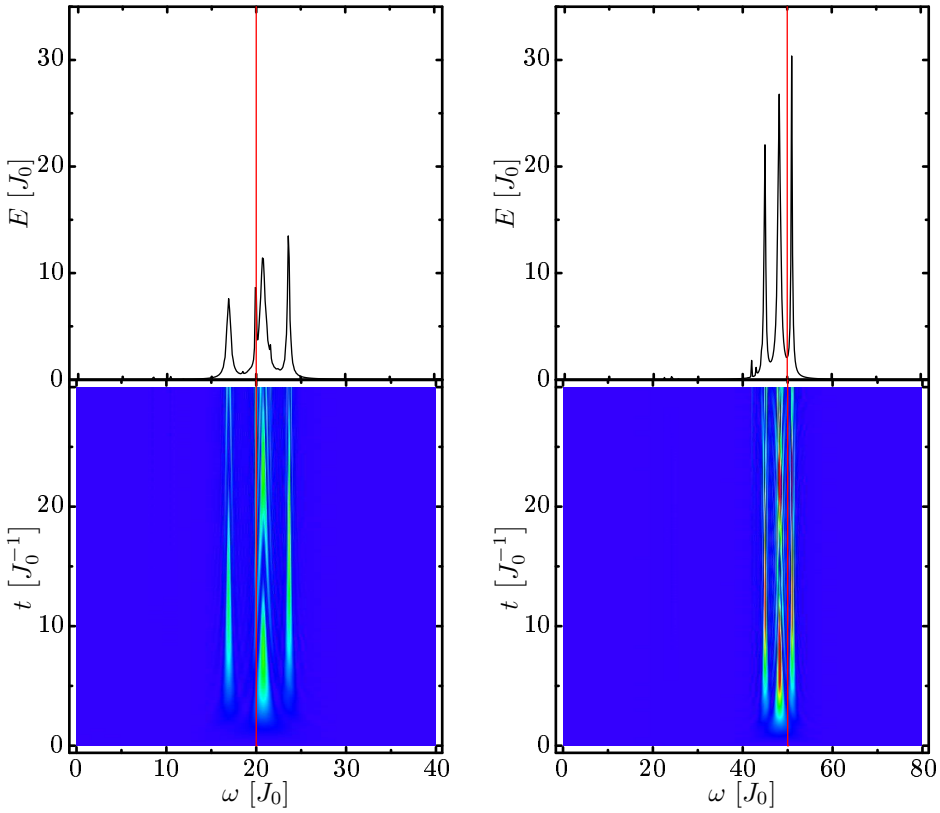

Figure 5.4: Energy transfer of a system of two fermionic species on 6 lattice sites. Each species contributes 3 atoms. Left hand side shows the system at the ratio $U_{\mathrm{cd}}/J_0 = 20$, right hand side at $U_{\mathrm{cd}}/J_0 = 50$. Depicted is the energy transfer as function of time and modulation frequency ω_{mod} (density plots in the lower row) and the time-averaged energy transfer over the whole simulation. The red line denotes the resonance frequency $\omega_{\mathrm{mod}} = U_{\mathrm{cd}}$.

particle-hole excitations.

The Fermi gas simulated with the ratios U_{cd}/J (figure 5.4) shows also very weak resonances for the modulation frequency $\omega_{\mathrm{mod}} = U_{\mathrm{cd}}/2$, which indicates the absorbtion of two photons of the corresponding energy.

Bibliography

[1] F. Dalfovo, St. Giorgini, L. P. Pitaevskii, S. Stringari; *Theory of Bose-Einstein Condensation in Trapped Gases*; Rev. Mod. Phys. **71** (1999) 463.

[2] M. H. Anderson, J. R. Ensher, M. R. Matthews, *et al.*; *Observation of Bose-Einstein Condensation in a Dilute Atomic Vapor*; Science **269** (1995) 198.

[3] K. B. Davis, M. O. Mewes, M. R. Andrews, *et al.*; *Bose-Einstein Condensation in a Gas of Sodium Atoms*; Phys. Rev. Lett. **75** (1995) 3969.

[4] D. Jaksch, C. Bruder, J. I. Cirac, *et al.*; *Cold Bosonic Atoms in Optical Lattices*; Phys. Rev. Lett. **81** (1998) 3108.

[5] M. Greiner, O. Mandel, T. Esslinger, *et al.*; *Quantum phase transition from a superfluid to a Mott insulator in a gas of ultracold atoms*; Nature **415** (2002) 39.

[6] K. Braun-Munzinger, J. A. Dunningham, K. Burnett; *Excitations of Bose-Einstein condensates in optical lattices*; Phys. Rev. A **69** (2004) 053613.

[7] Thilo Stöferle, Henning Moritz, Christian Schori, *et al.*; *Transition from a Strongly Interacting 1D Superfluid to a Mott Insulator*; Phys. Rev. Lett. **92** (2004) 130403.

[8] Neil W. Ashcroft; *Festkoerperphysik*; Oldenbourg (2001).

[9] F. Gebhard; *The Mott Metal-Insulator Transition*; Springer Tracts (1997).

[10] R. Roth, K. Burnett; *Superfluidity and Interference Pattern of Ultracold Bosons in Optical Lattices*; Phys. Rev. A **67** (2003) 031602(R); e-Print: **cond-mat/0209066**.

[11] G. G. Batrouni, R. T. Scalettar; *World-line quantum Monte Carlo algorithm for a one-dimensional Bose model*; Phys. Rev. B **46** (1992) 9051.

[12] J. K. Freericks, H. Monien; *Strong-coupling expansion for the pure and disordered Bose-Hubbard model*; Phys. Rev. B **53** (1996) 2691.

[13] O. Penrose, L. Onsager; *Bose-Einstein Condensation and Liquid Helium*; Phys. Rev. **104** (1956) 576.

[14] M. Greiner, C. A. Regal, D. S. Jin; *Probing the excitation spectrum of a Fermi gas in the BCS-BEC crossover regime*; Phys. Rev. Lett. **94** (2005) 070403.

[15] M.W. Zwierlein, J.R. Abo-Shaeer, A. Schirotzek, *et al.*; *Vortices and superfluidity in a strongly interacting Fermi gas*; Nature **435** (2005) 0358.

[16] E. Tiesinga, B. J. Verhaar, H. T. C. Stoof; *Threshold and resonance phenomena in ultracold ground-state collisions*; Phys. Rev. A **47** (1993) 4114.

[17] Michael Köhl, Henning Moritz, Thilo Stöferle, *et al.*; *Fermionic atoms in a 3D optical lattice: Observing Fermi-surfaces, dynamics and interactions*; Phys. Rev. Lett. **94** (2005) 080403.

[18] Karen Braun-Munzinger; *Dynamics of Bose-Einstein condensates in optical lattices*; Ph.D. thesis; University of Oxford (2005).

[19] J. Stenger, S. Inouye, A. P. Chikkatur, *et al.*; *Bragg Spectroscopy of a Bose-Einstein Condensate*; Phys. Rev. Lett. **82** (1999) 4569.

[20] M. Köhl, H. Moritz, T. Stöferle, *et al.*; *Superfluid to Mott insulator transition in one, two, and three dimensions*; Journal of Low Temperature Physics **138** (2005) 635.

[21] Gordon Baym, C. J. Pethick; *Ground-State Properties of Magnetically Trapped Bose-Condensed Rubidium Gas*; Phys. Rev. Lett. **76** (1996) 6.

[22] Tim Davis; *UMFPACK V4.3, an unsymmetric-pattern multifrontal method*; ACM Transactions on Mathemathical Software **30** (2004) 196.

[23] URL `http://www.computational.unibas.ch/cs/scicomp/software/pardiso/`.

[24] William H. Press, Saul A. Teukolsky, William T. Vetterling, Brian P. Flannery; *Numerical Recipes in C*; Cambridge University Press; second edn. (1995).

[25] E. Fehlberg; *Low-order classical Runge-Kutta formulas with stepsize control and their application to some heat transfer problems*; NASA Technical Report **315** (1969) 28.

[26] J.R. Cash, A.H. Karp; ACM Transactions on Mathemathical Software **16** (1990) 201.

Danksagung

An erster Stelle möchte ich Prof. Dr. Robert Roth für die Möglichkeit zur Anfertigung dieser Arbeit danken, wie auch für sein anhaltendes Interesse und seine motivierende Art während meiner gesamten bisherigen Zeit in der Gruppe.

Dank gebührt vor allem meinem Kommilitonen Felix Schmitt, der immer für fachliche und ausser-fachliche Gespräche ein offenes Ohr hat, und wesentlich zum Verständnis unseres Arbeitsgebietes beigentragen hat.

Der gesamten Theorie-Abteilung des Instituts für Kernphysik möchte ich für freundliche und angenehme Atmosphäre danken. Dank geht hier besonders an die *Kaffeerunde*– David Ondreka, Thomas Roth, Mathias Wagner und Verena Werth.

Clemens Kruspel danke ich dafür, dass er sich als Nicht-Physiker diese Arbeit zur Korrektur gelesen hat, und als Freund immer verfügbar ist.

Ich danke Tinka Spehr und meiner Mitbewohnerin Julia Hahn dafür, das sie immer als Freunde da sind.

Dank geht an die Mitglieder der Keith Burnett Theory Group (Oxford) sowie Dr. Karen Braun-Munzinger für ihre fachliche Unterstützung.

Besonderer Dank geht an meine Mutter Lieselotte Hild und meinen Bruder Michael, für die anhaltende, bedingungslose und unermüdliche Unterstützung in jeglicher Hinsicht während meines Studiums.

Erklärung zur Diplomarbeit gemäß §19 Abs. 6 DPO/AT

Hiermit versichere ich, die Diplomarbeit ohne Hilfe Dritter nur mit den angegebenen Quellen und Hilfsmitteln angefertigt zu haben. Alle Stellen, die aus diesen Quellen entnommen wurden, sind als solche kenntlich gemacht worden. Diese Arbeit hat in gleicher oder ähnlicher Form noch keiner Prüfungsbehörde vorgelegen.

Darmstadt, den 18. Juli 2005

Markus Hild